ANKARA YILDIRIM BEYAZIT UNIVERSITY

GRADUATE SCHOOL OF NATURAL AND APPLIED SCIENCES

INVESTIGATION OF ELECTROLESS SILVER PLATING PROCESS ON $0.68CaTiO_3$-$0.32Ca(Zn_{1/3}Nb_{2/3})O_3$ CERAMIC COMPOSITION

M.Sc. Thesis by

Kardelen GÜNDOĞDU

Department of Materials Engineering

October, 2023

ANKARA

INVESTIGATION OF ELECTROLESS SILVER PLATING PROCESS ON $0.68CaTiO_3$-$0.32Ca(Zn_{1/3}Nb_{2/3})O_3$ CERAMIC COMPOSITION

A Thesis Submitted to

The Graduate School of Natural and Applied Sciences of

Ankara Yıldırım Beyazıt University

In Partial Fulfillment of the Requirements for the Degree of Master of Science

in Materials Engineering, Department of Materials Engineering

by

Kardelen GÜNDOĞDU

October, 2023

ANKARA

M.Sc. THESIS EXAMINATION RESULT FORM

We have read the thesis **entitled "INVESTIGATION OF ELECTROLESS SILVER PLATING PROCESS ON $0.68CaTiO_3$-$0.32Ca(Zn_{1/3}Nb_{2/3})O_3$ CERAMIC COMPOSITION"** completed by **KARDELEN GÜNDOĞDU** under the supervision of **ASSOC. PROF. DR. METEHAN ERDOĞAN** and we certify that in our opinion it is fully adequate, in scope and in quality, as a thesis for the degree of Master of Science.

Assoc. Prof. Dr. Metehan ERDOĞAN

Supervisor

Prof. Dr.	Asst. Prof. Dr.
İshak KARAKAYA	Begüm ÜNVEROĞLU ABDİOĞLU
Jury Member	Jury Member

Prof. Dr. Sadettin ORHAN

Director

Graduate School of Natural and Applied Sciences

ETHICAL DECLARATION

I hereby declare that, in this thesis which has been prepared in accordance with the Thesis Writing Manual of Graduate School of Natural and Applied Sciences,

- All data, information and documents are obtained in the framework of academic and ethical rules,
- All information, documents and assessments are presented in accordance with scientific ethics and morals,
- All the materials that have been utilized are fully cited and referenced,
- No change has been made on the utilized materials,
- All the works presented are original,

and in any contrary case of above statements, I accept to renounce all my legal rights.

Date: **Signature:**……...

Name & Surname:…….

ACKNOWLEDGMENTS

I would first like to thank my thesis advisor Assoc. Prof. Dr. Metehan Erdoğan for his guidance, suggestions, and support throughout my thesis period. I also wish to express my gratitude to Prof. Dr. Cihangir Duran and Prof. Dr. İshak Karakaya.

Many thanks goes to Research Assistant Uğur Barut, Research Assistant Oğuzhan Bilaç and Hasan Tahsin Koç for helping and supporting me in characterization part of my thesis.

My special thanks goes to Esra Sütcü, Olgun Yılmaz, Atalay Balta, Seda Kartal, İshak Emre Ömür, Aybike Nur Çardaktan Yalçın, Mertcan Başkan, and the METU-TEMPLAB team who supported me morally in all the studies I carried out to complete my thesis.

I am deeply thankful to my family especially my dear father, mother and brother for supporting me continuous encouragement throughout my life. I would like to express my very profound gratitude to Berkay Çağan for supporting and continuous encouraging with his love.

2023, 27 September **Kardelen GÜNDOĞDU**

INVESTIGATION OF ELECTROLESS SILVER PLATING PROCESS ON $0.68CaTiO_3$-$0.32Ca(Zn_{1/3}Nb_{2/3})O_3$ CERAMIC COMPOSITION

ABSTRACT

Coating technology is carried out to provide corrosion, conductivity, decrease surface friction and aesthetic benefits. Silver plating is carried out with or without electricity, but it is possible to make homogeneous coating on both metallic and non-metallic substrates that have complex geometry with electroless silver plating. In the scope of this study, optimization of electroless silver plating was studied on catalytically inactive 0.68 mole fraction of calcium titanate and 0.32 mole fraction calcium zirconium niobate resonator ceramic systems. An electroless silver plating bath was optimized along with the pretreatment processes, and two-stage metallization was applied to rough surfaces obtained after 5 percent hydrofluoric acid etching. The ceramics were immersed in three different coating baths after palladium activation. Surface morphology, elemental analysis, phase formation, and coating thickness were analyzed using scanning electron microscopy, energy dispersive spectroscopy, x-ray diffraction, and x-ray fluorescence from the top and cross-section of samples. The optimum metallization procedure were determined for sensitization and palladium baths, and the maximum coating thickness, 13.46 micrometers, was obtained after 1 hour with the addition of 20 milliliters of ethylenediaminetetraacetic acid at 60 degrees Celsius.

Keywords: Electroless coating, electroless silver coating, metallization, calcium titanate-based resonator ceramics

$0.68CaTiO_3$-$0.32Ca(Zn_{1/3}Nb_{2/3})O_3$ SERAMİK KOMPOZİSYONU ÜZERİNE AKIMSIZ GÜMÜŞ KAPLAMA PROSESİNİN İNCELENMESİ

ÖZ

Kaplama teknolojisi korozyon direnci, iletkenlik, yüzey sürtünmesinin azaltılması ve estetik fayda sağlamak amacı ile uygulanır. Gümüş, akımlı veya akımsız yöntemler ile yüzey üzerine biriktirilebilinir fakat akımsız gümüş kaplama ile hem iletken hem de iletken olmayan kompleks geometriye sahip altlık malzemeler homojen kaplanabilir. Bu çalışma kapsamında, katalitik olarak aktif olmayan 0.68 mol fraksiyonlu kalsiyum titanat ve 0.32 mol fraksiyonlu kalsiyum zirkonyum niobat rezonatör seramik sistemleri üzerinde akımsız gümüş kaplama optimizasyonu çalışılmıştır. Ön işlem süreçleri ile birlikte akımsız gümüş kaplama banyosu optimize edilmiş ve yüzde 5 hidroflorik asit dağlamasının ardından elde edilen pürüzlü yüzeylere iki aşamalı metalizasyon prosedürü uygulanmıştır. Paladyum aktivasyonundan sonra seramikler üç farklı kaplama banyosuna daldırılmıştır. Yüzey morfolojisi, element analizi, faz oluşumu ve kaplama kalınlığı numunelerin üst ve enine kesitlerinden taramalı elektron mikroskobu, enerji dağılımlı spektroskopi, x-ışını kırınımı ve x-ışını flor ışıması ile analiz edilmiştir. Sensitizasyon ve aktivasyon banyoları için optimum metalizasyon prosedürleri belirlenmiş, maksimum kaplama kalınlığı,13.46 mikrometre, 60 santigrat derecede 20 mililitre etilendiamintetraasetik asit ilavesi içeren akımsız gümüş kaplama banyosu ile 1 saat sonunda elde edilmiştir.

Anahtar Kelimeler: Akımsız kaplama, akımsız gümüş kaplama, metalizasyon, kalsiyum titanat bazlı rezonatör seramikler

CONTENTS

NOMENCLATURE

Roman Letter Symbols

E	Reduction potential
$E^{1/2}$	Half reduction potential
M	Metal ion
Q	Q factor
R	Reducing agent ion
T	Absolute temperature, °C
V	Voltage, V

Greek Letter Symbols

$\mathring{A}$	Angstrom
α	Activity
ε_r	Relative permittivity
λc	Free space wavelength
λg	Dielectric wavelength
μm	Micrometer
$tan\ \delta$	Dielectric loss
τ_ε	Temperature dependence of relative permittivity
τ_f	Near zero temperature coefficient of resonant frequency

Subscripts

f	Frequency
G	Glass
h	Hour
min	Minute
W_d	Dry Weight
W_s	Suspended Weight
W_w	Wet Weight

Abbreviations

at. %	Atomic percent
cm	Centimeter

GHz	Gigahertz
mPa	MegaPascal
nm	Nanometer
ppm	Parts per million
wt. %	Weight percent

Acronyms

AP	Apparent Porosity
B1	Electroless silver plating bath 1
B2	Electroless silver plating bath 2
B3	Electroless silver plating bath 3
BD	Bulk Density
CR	Cavity resonator
CT	$CaTiO_3$
CT-CZN x32	$0.68CaTiO_3$-$0.32Ca(Zn_{1/3}Nb_{2/3})O_3$
CZN	$Ca(Zn_{1/3}Nb_{2/3})O_3$
DM	Digital microscope
DMAB	Dimethyl amine borane
DR	Dielectric resonator
DRA	Dielectric resonator antenna
EDS	Energy dispersive spectrometry
EDTA	Ethylenediaminetetraacetic acid
GPS	Global positioning system
HF	Hydrofluoric acid
JCPDS	Joint committee on powder diffraction standards
LR	Line resonator
LTCC	Low temperature co-firing ceramics
OM	Optical microscope
PP	Polypropylene
P1	Activation bath 1
P2	Activation bath 2
Qxf	Quality factor
SEM	Scanning electron microscope
SHE	Standard hydrogen electrode

SiC	Silicon carbide
S1	Sensitization bath 1
S2	Sensitization bath 2
WA	Water Absorption
XRD	X-Ray diffraction
XRF	X-Ray fluorescence

LIST OF TABLES

LIST OF FIGURES

CHAPTER 1

INTRODUCTION

1.1 Microwave Resonator Ceramics

Microwave dielectric materials are crucial for a wide range of wireless communication applications, including GPS [1], cellular phones [2] and radar systems [3]. Increasing demand for dielectric resonators (DRs), which are low-loss ceramic pucks that are used primarily in wireless communication devices, has resulted from advancements in microwave telecommunication, satellite broadcasting, and intelligent transport systems [4].

By reducing the size and cost of filters [5], oscillators [6], and antenna components [7] in applications ranging from mobile phones to global positioning systems, dielectric oxide ceramics have revolutionized the microwave wireless communications industry.

Systems that oscillate at higher frequencies are called resonators and this oscillation can be mechanical or electromagnetic [8]. Typically, a resonator generates waves at specific frequencies and filters them. Cavity resonator systems are a conductive closed system that contains a cavity in a metal block, where signals are reflected back and forth on the cavity walls [9]. Since the conductivity of walls are high, a high-quality factor (Q factor), which is a parameter that describes the resonance behavior of the resonator, is obtained in this type of resonator system.

In DR systems, when the porous material with a higher dielectric constant (i.e. ceramics) is surrounded by metal (i.e. silver, gold, copper, etc.) with a lower dielectric value and higher conductivity, electromagnetic energy is stored in the system with the sudden change in dielectric constant [10]. There are many types of dielectric resonators, but the most common is the ceramic disc, which has a low dissipation factor as well as a high permittivity. Physical dimensions and permittivity of the material and its immediate environment determine the resonant frequency of a disc.

1.1.1 History of Dielectric Resonator Systems

The term dielectric resonator was defined by Richtmyer in 1939 [11] , within the scope of this definition, it was shared that a suitable shaped of dielectric part can be used in microwave systems. After this definition within 20 years, Schlicke introduced standard ceramic capacitors with high relative permittivity and showed their poor application areas in radio frequency systems [12]. The relative permittivity and Q value of titanium dioxide were measured in the microwave frequency range at room temperature by Okaya and Barash in 1962 [13]. As a result of the ongoing studies on dielectric resonators, the first microwave resonator filter was created from a rutile single crystal in 1968, by carrying out experimental and theoretical studies for the first time by Cohen et.al. from Rantec Corporation. Although TiO_2 immediately met criteria for high relative permittivity and low dielectric loss, its temperature stability is poor ($\tau f \sim$ +450 ppm/°C). However, he shared the knowledge that dielectric resonator systems have dielectric constants that vary according to temperature compared to conventional systems. For example, the dielectric constant change for TiO_2 was measured as 1000 ppm/°C, which leads to a frequency change of 500 ppm/°C [14].

In the early 1970s, the first $BaTi_4O_9$ low-loss ceramic was produced by Masse et al.[15]. After that, the $Ba_2Ti_9O_{20}$ ceramic system developed in Bell laboratory was reported with its improved features like high temperature stability (τf 0-2) and high Q factor values [16]. The $BaTiO_3$-Ln_2O_3-TiO_2 system investigated by Bolton with a low loss temperature-stable ceramic system with high relative permittivity [17]. Solid solutions of $MgTiO_3$-$CaTiO_3$, zirconium-tin with titanium (IV) oxide (ε_r = 34-37), and $BaTi_4O_9$ (ε_r = 34-37) were developed [18]. Miniaturization in dielectric resonator systems started in 1975 and commercial production began approximately five years later [19]. Moreover, compositions of ceramics that were used as resonators in microwave applications are given in Table 1.1.

Plourde and Ren determined the Q factor (Q = 8000-10000 at 4GHz and ε_r = 40) [20] in 1981, which is one of the critical parameters of the $Ba_2Ti_9O_{20}$ composition. They started their first studies in 1970 [20].

Table 1.1 Examples of resonators in microwave applications. Reproduced from [10].

Ceramic Composition	ε_r	Q (GHz)	τ_f
$Ba_2Ti_9O_{20}$	40	8000-10000 (at 4GHz)	2
$SnTiO_4$ or $ZrTiO_4$	34-37	8000-10000 (at 4GHz)	20
$BaTi_4O_9$	38	7000-10000 (at 4GHz)	15

According to Ian M. Reaney and David Iddles's article that published in 2006, invar air cavities were used in resonator filter systems at base stations. Ceramic resonators became popular in these areas in the 1980s, and in the 1990s, they became common in base stations as well [2]. Ceramic dielectric resonator systems have become increasingly popular over the years due to their advantages. Based on Figure 1.1, the number of published papers in this field has increased over the years, and studies were conducted to meet the dielectric properties of various applications.

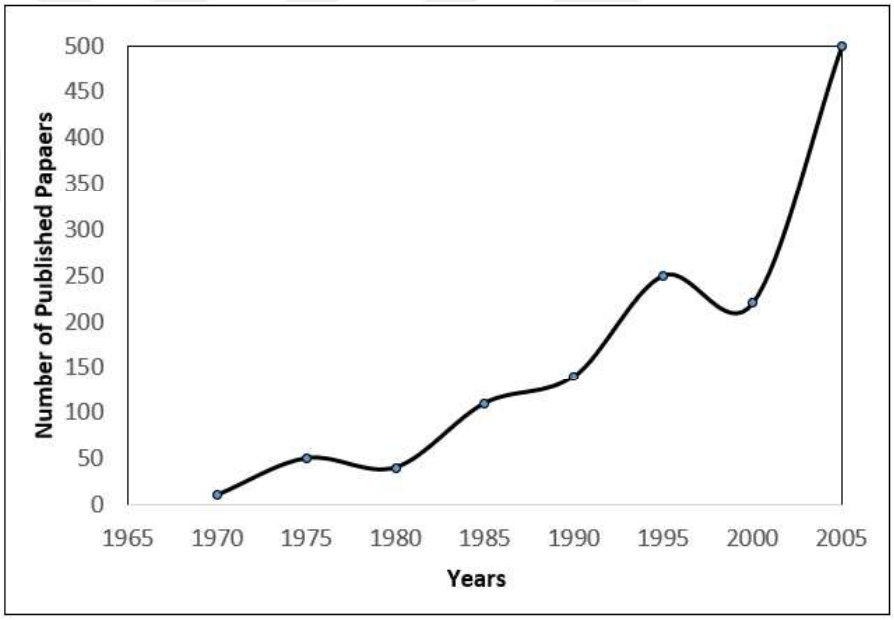

Figure 1.1 Number of published papers in 1965-2005. Reproduced from [10].

Understanding microwave ceramic's relationship between structure and properties has been enhanced in recent years, and new materials with a higher permittivity, better temperature stability, and a much lower sintering temperature have been developed. In

addition to developing new microwave devices such as oscillators, antennas, and band-pass filters, co-fired multilayer devices are now possible [21].

1.1.2 Important Parameters

Passive microwave devices can be significantly miniaturized using ceramics with high permittivity. Temperature-stable resonators require ceramics with high relative permittivity (ε_r), low dielectric losses (tan δ), a near zero temperature coefficient of resonant frequency (τ_f), and high Q factor [6].

In general, the relative permittivity (ε_r) should be as large as possible, since the size of a resonator is inversely proportional to its square root approximately $20 < \varepsilon_r < 100$. In the microwave frequency range, free space wavelength (λc) is in centimeters and hence the wavelength (λg) inside the dielectric will be in millimeters only when the value of ε_r is in the range 20–100, as can be seen from Equation (1.1). To get resonance, dimensions of the dielectric must be of the same order (in millimeters) [18].

$$\lambda_g = \frac{\lambda_c}{\sqrt{\varepsilon_r}} \qquad \textbf{(1.1)}$$

The dielectric losses (tan δ) should be as small as possible to obtain a high Q value [6] as deduced from Equation (1.2). However, Q is not an independent parameter, since experience has shown that the product of Q and the resonant frequency (f_o) is approximately constant. It is therefore important to refer to the measurement (resonant) frequency when referring to the Q value of materials. Today, Q > 30,000 at 1 GHz is essential for many practical applications [18]. Based on the resonator types and operation frequencies, Figure 1.2 illustrates the classification of resonators.

The resonator should have a resonant frequency coefficient of + 2ppm/°C to ensure temperature stability. Cations can be substituted into the base composition if it is not temperature stable until $\tau f \sim 0$ is achieved. An increase in polarizability results in an increase in relative permittivity when the substitution occurs [18].

$$Q = \frac{1}{tan\delta} \quad \textbf{(1.2)}$$

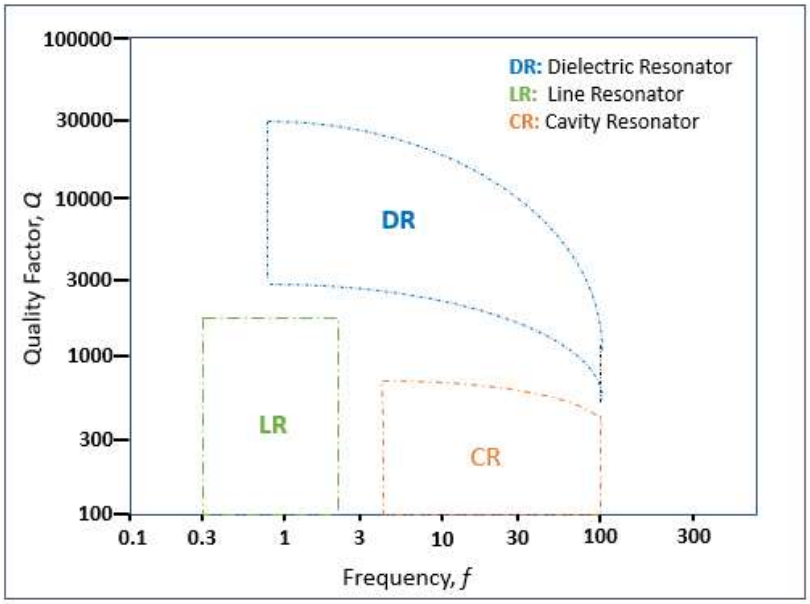

Figure 1.2 Classification of resonators according to operating frequencies and quality factors. Reproduced from [6].

Larger ε_r provides greater energy condensing, reduced radiation losses, and better miniaturization. At the same time, larger ε_r will cause higher dielectric losses because of inherent material properties. A DR that is properly fed can also radiate microwave energy when exposed to free space, which is why it is referred to as a Dielectric Resonator Antenna (DRA) [10].

Also, number of parameters affect microwave ceramic properties, such as purity of starting powder, calcination temperature, shaping technique (dry pressing, tape casting, gel casting), and sintering temperature and heating/cooling rate as well [10].

Based on the dielectric properties and relative density, Figure 1.3 shows the calcination temperature of the Ba ($Sm_{1/2}$ $Nb_{1/2}$) ceramic composition. A high relative density is dependent on the purity of the starting powder and the ceramic production method. While the relative permittivity also reaches 98%, τf moves away from zero that expected to be close to zero, and *Qxf* decreases.

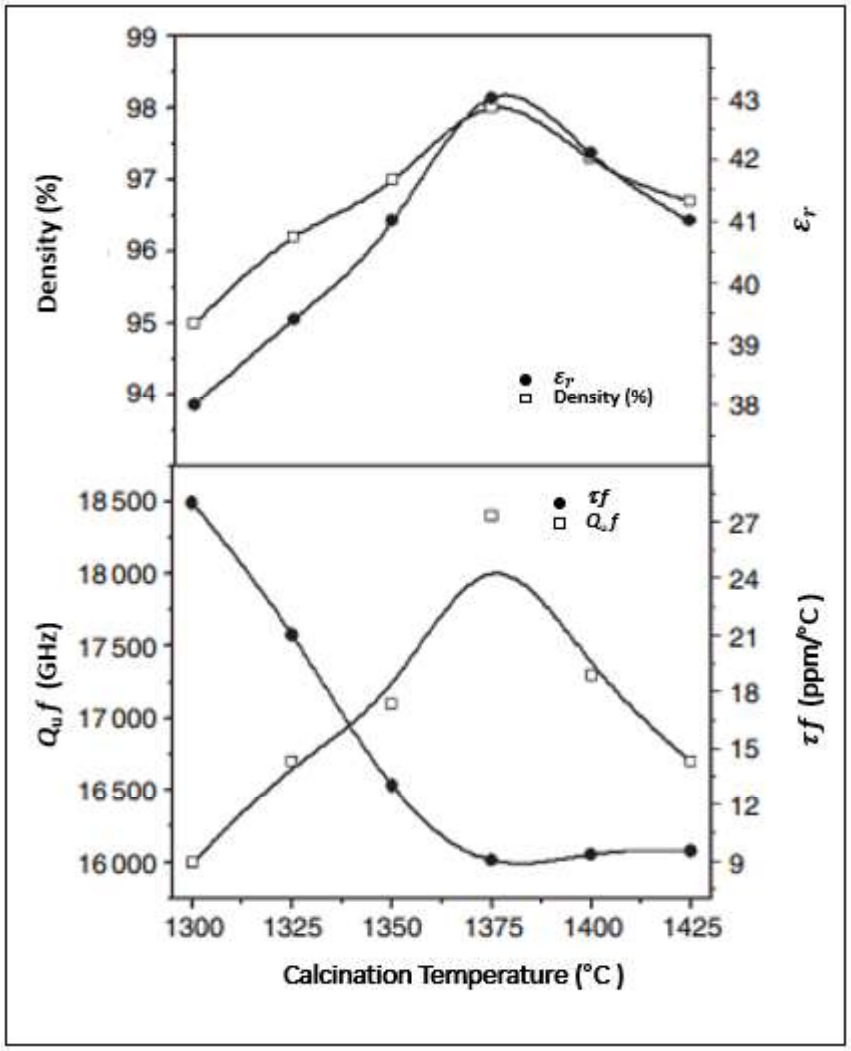

Figure 1.3 Effect of calcination temperature on density and microwave dielectric properties. Reproduced from [10].

1.1.3 Application Areas

Dielectric ceramics have high Q outputs, despite their high cost, which makes them ideal for microwave resonator systems. Multi-mode resonance can also be induced by a variety of geometry [22]. Besides microwave dielectric ceramics used in base stations [23], and military search radars in X band resonator antennas [24], LTCC applications [25], tunable filters [26], and high-frequency applications [27] are also common. Ceramic microwave dielectrics play a crucial role in mobile systems. Current microwave systems require new designs, improved dielectric materials, and improved microwave components. Microwave communication systems have been

revolutionized by the use of dielectric oxide ceramics as filters and oscillators in applications such as mobile phones and global positioning systems [28]. DRs at mobile telephone base stations ensure high-quality primary signals with minimal interference by removing unwanted sidebands and secondary signals [18]. As shown in Figure 1.4, microwave dielectric materials evolve as a function of quality factor (Qxf) and dielectric constant (ε_r). For millimeter wave communication as well as microwave integrated circuits, ceramics with low dielectric constants are the preferred substrate. Base stations for cell phones and satellite communications use ceramics with high dielectric constants between 25 and 150. It is preferred to use ceramics of the tungsten-bronze type with high dielectric constants for mobile phones because they allow the device to miniaturize.

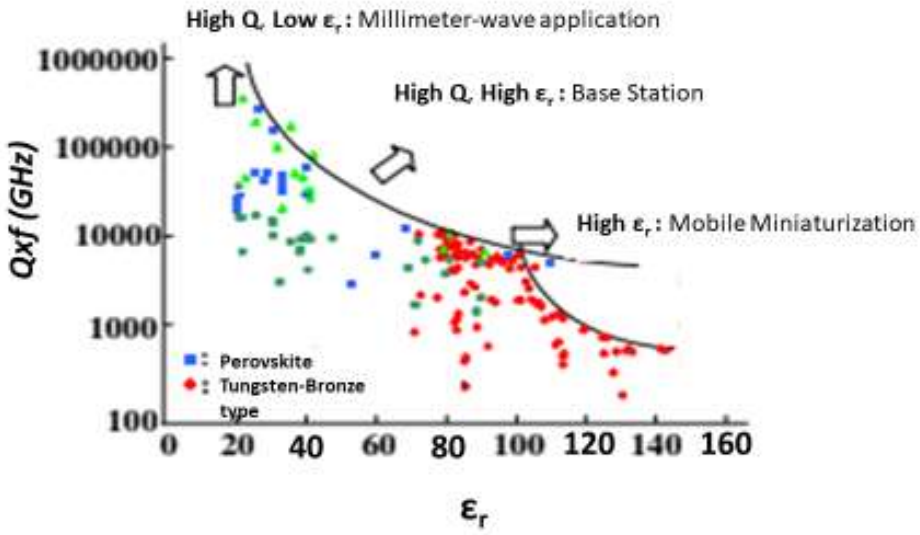

Figure 1.4 Example of microwave dielectric ceramics application areas and requirements. Reproduced from [29].

1.2 Ca-Based Ceramic Systems

It is essential that a full understanding of oxide ceramic crystal chemistry is developed in order to advance these microwave circuits [10]. A material with the desired properties can obtain by combining two dielectrics with different relative permittivity or temperature dependence. The Liechtenecker logarithmic rule relates the volume

fractions 1 – x and x and the relative permittivity of ε_1 and ε_2 of the two components to the final relative permittivity ε' [18]:

$$\log \varepsilon' = (1 - x) \log \varepsilon_1 + x \log \varepsilon_2 \quad \textbf{(1.3)}$$

The equivalent relationship for the temperature dependence of relative permittivity (τ_ε) for a material resulting from components (1) and (2) is [18]:

$$\tau_\varepsilon = (1 - x)\tau_\varepsilon (1) + x\, \tau_\varepsilon (2) \quad \textbf{(1.4)}$$

In ceramics, non-monotonic mixture behavior can be defined as $A^{2+}B^{4+}O_3$ and $A^{2+}(B_1^{2+}\, B_2^{5+})O_3$ or $A^{2+}\,(B_1^{2+}\, B_2^{5+}\,)O_3$ -type ceramics. $CaTiO_3$–$Ca(Zn_{1/3}\, Nb_{2/3})O_3$ [30], $CaTiO_3$–$Ca(Mg_{1/3}\, Nb_{2/3})O_3$ [31], $CaTiO_3$–$Pb(Fe_{1/2}\, Nb_{1/2})O_3$ [32] are examples of this system.

$CaTiO_3$ has a high ε_r of 170 and a moderate *Qxf* of 3600 GHz, and is regarded as an exciting material for microwave applications [33]. However, its τf value is 800 ppm/°C and this limits its application in thermal stability [34]. A crystal phase transformation from cubic to tetragonal occurs at 1307°C during cooling. When the tetragonal phase reaches 1227°C, it changes into the orthogonal phase [18].

Mixing two compounds with positive and negative temperature coefficients can produce a suitable ceramic by forming a solid solution or mixture phase that has zero temperature coefficient of the resonant frequency. It is possible to categorize mixed ceramic approaches into three categories; (i) Anomalous behavior, (ii) Linear change and (iii) Non-monotonic mixture-like behavior [30].

Microwave dielectric ceramic compositions based on $CaTiO_3$ (CT) with dielectric constant in the range of 23-150 are shared in Appendix A. When $(1\text{-}x)CaTiO_3$-$(x)Ca(Zn_{1/3}Nb_{2/3})O_3$ ceramic compositions with dielectric constant given in Table 1.2 are examined; CT composition with ε_r=170 and *Qxf* value of 3600 GHz (see in Table 1.2) reaches higher Q values when mixed non-monotonically.

Table 1.2 Microwave dielectric properties of CT-Like ceramics.

Composition	ε_r	*Qxf* (GHz)	τ_f	Sintering Parameters	Ref.
$0.8CaTiO_3$-0.2 $Ca(Zn_{1/3}Nb_{2/3})O_3$	115	5030	336	1400°C for 4h	[30]
$0.6CaTiO_3$-0.4 $Ca(Zn_{1/3}Nb_{2/3})O_3$	76	7560	164	1400°C for 4h	[30]
$0.4CaTiO_3$-0.6 $Ca(Zn_{1/3}Nb_{2/3})O_3$	62	9540	25	1350°C for 4h	[30]
$0.3CaTiO_3$-0.7 $Ca(Zn_{1/3}Nb_{2/3})O_3$	76	10860	-6	1350°C for 4h	[30]
$0.2CaTiO_3$-0.8 $Ca(Zn_{1/3}Nb_{2/3})O_3$	42	13030	-28	1350°C for 4h	[30]
$CaTiO_3$	170	3600	800	-	[33]

1.3 Purpose of the Study

Electronic devices are constantly decreasing in dimensions today. When size increases, the permittivity of material decreases, so the demand for resonator systems with high permittivity (ε_r) has increased with device miniaturization [35]. In resonator systems, Richtmyer proposed the use of a solid dielectric instead of an air-filled metal cavity [36].

Due to the low losses expected from microwave resonator ceramics, which also used in LTCC, filters, and radar systems, they must completely be covered with a highly conductive metal. The high conductivity of silver makes it a preferred metal in ceramics. At microwave frequencies the best conducting material with the lowest resistivity now becomes silver, due to its lowest inter-band transitions being in the UV (308 nm) [37]. Silver ensures excellent Q, good solderability, and adhesion. Moreover, high signal transitions ensured and signal losses prevented. [38].

Electrical resistivity is inversely proportional with conductivity, so with higher conductivity, high current load can be obtained while reducing loss at highest

frequencies and this is important for attaining reduced levels of passive intermodulation application [39].

In either case, after the substrate material has been pretreated, silver deposits with or without electricity. Silver paste application is preferentially applied for mass production in order to make the surface conductive and to perform dielectric measurements [35-40,41]. It is possible to make homogeneous coating with electroless silver coating on metallic or non-metallic materials with complex geometry. Electroless metal coating refers to the deposition of a metal on a conductive, semiconductor or non-conductive substrate by chemical methods without the need for an electrical source [42].

Electroless silver plating is classified into two within the scope of substituting and reduction of metal ions as shown in Figure 1.5. While better stabilization is achieved with the substituting of metal ions, there is a limitation of coating thickness [43]. In the silver-plating process, which takes place with reduction reactions, a water-soluble silver compound reduces to metallic silver with the reducing agent in the bath and precipitates on the sample surface as illustrated in Figure 1.6.

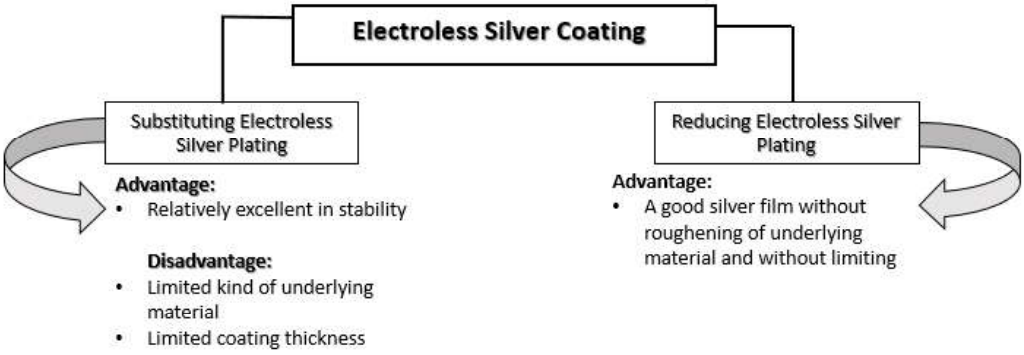

Figure 1.5 Classification of electroless silver plating. Reproduced from [43].

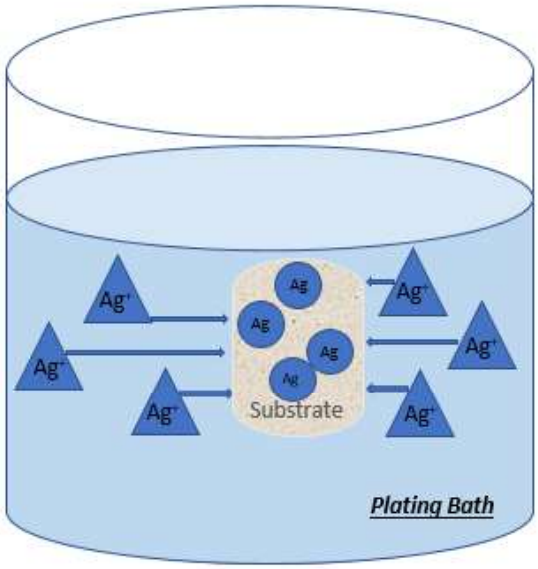

Figure 1.6 Schematic illustration of reducing electroless silver plating solution. Reproduced from [44].

The main purpose of this study is to obtain a high conductivity value by electroless silver coating on the catalytically inactive ε_r =89.6 0.68$CaTiO_3$-0.32$Ca(Zn_{1/3}Nb_{2/3})O_3$ (CT-CZN x32) microwave resonator ceramics. Understanding the background information of electroless silver plating includes an innovative approach in terms of applicability and defining the mechanism of this process, which is necessary for the defense industry to start mass production on a large scale, due to its advantages.

The process sequence of electroless silver coating includes original etching, cleaning, and metallization steps. The schematic representation of pretreatment processes of electroless silver plating is given in Figure 1.7. With the metallization process, nucleation zones are formed on the surface, thus making it easier for the coating to adhere to the surface. In this context, CT-CZN x32 ceramics with high relative density and low open porosity were produced by tape-casting. The ceramic composition was analyzed with XRF and it was aimed to precipitate silver ions by forming catalytic Pd sites after roughening the surface without damaging it. Furthermore, electroless silver bath was optimized by experiments at different temperatures and concentrations.

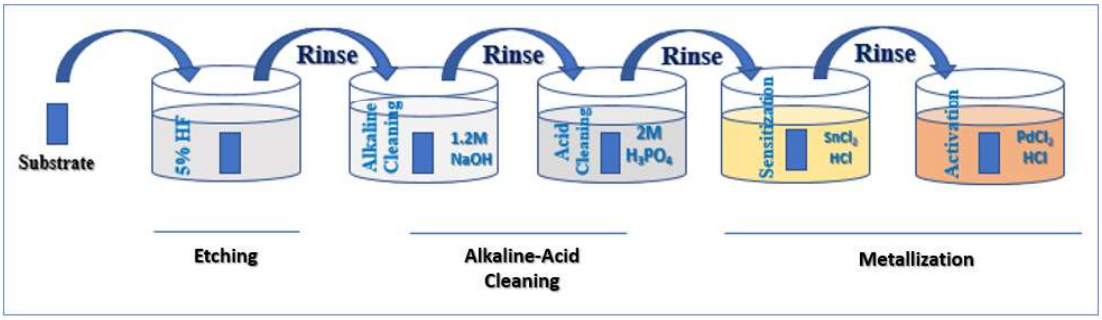

Figure 1.7 Schematic representation of pretreatment processes before electroless silver plating.

CHAPTER 2

LITERATURE REVIEW

2.1 Fundamental Concepts of Silver Electrochemistry

Silver is a metal with the highest electrical conductivity of all metals as seen in Table 2.1). In addition, silver which has a highly cathodic standard electrode potential ($E_{Ag+/Ag}$ = 0.79 V vs SHE) [45], is surpassed in terms of nobility only by gold and platinum group metals. As seen in Figure 2.1, the silver Pourbaix diagram shows that at potentials below about 0.4 V and in the absence of complexing ions, silver is immune to reaction over nearly the entire pH range [46].

Table 2.1 Approximate electrical resistivity of selected materials at 25°C. Reproduced from [47].

Metal	Resistivity x10^{-8} (Ωm)
Ag	1.48
Cu	1.56
Au	2.04
Al	4.29
Zn	5.49
Ni	6.097
Cd	6.80
Fe	8.92
Pt	9.8
Pd	10.75
Sn	11.49
Cr	12.658
Pb	18.867
Ti	43.478
Hg	100

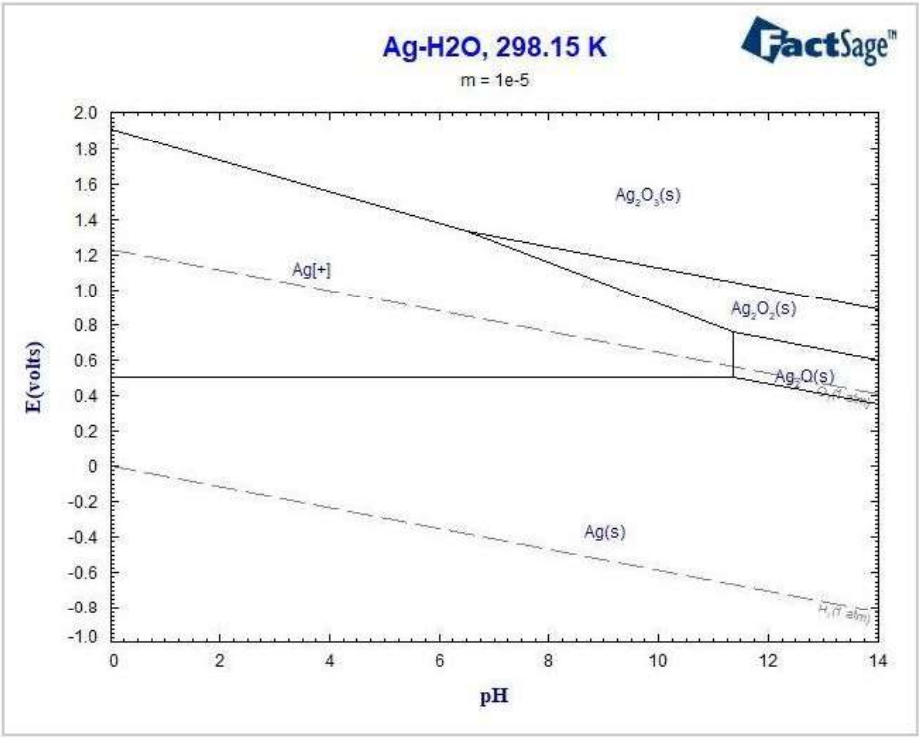

Figure 2.1 Pourbaix diagram for silver at room temperature.

Electrochemical nobleness can be defined with half-reactions ($M^+ + e^- \rightarrow M^0$ or $M^{2+} + 2\ e^- \rightarrow M^0$) in the M^+ and M^{2+} oxidation state [48]. According to this scope, gold has the highest $E^{½}$ = + 1.7 V, followed by + 0.79 V for Ag and + 0.5 V for Cu.

In general applications, silver is more noble than the metal on which it is coated and therefore tends to form 'immersion deposits' [49]. Silver plating is widely used in solderable surfaces, electrical contact applications, high electrical and thermal conductivity required applications, thermo-compression bonding and wear resistance requirements of load-bearing surfaces [50]. Even if silver plating was preferred in decorative applications such as tableware in the past, it is mostly preferred in electronic applications due to its high conductivity values, recently. Silver plating is also used in the semiconductor chip manufacturing industry. Silvered lead frames [51] reduced the loss of performance together with the conductivity values that silver provides at the highest level, and at the same time, it allows for less costly work as it is preferred instead of gold. However, in the long term, in applications that require electrical

contact, the oxides, and sulfides, which form on the surface over time, are also disadvantageous due to the increase in contact resistance [52].

Silver has high wear resistance and load-bearing surface applications have been available for many years [53]. Also, due to its solderability feature, silver coating is also used in bus bars [54] and intermediate-frequency housing applications [55]. Waveguides [56], switch components [57], and connector pins [58] are also application areas for silver plating.

In 1800, a paper published about silver plating by Professor Brugnatelli (the University of Pavia, Chemistry Department), after which the first patent was obtained in 1840 [59] for a cyanide-containing silver plating bath [60]. However, due to the toxicity of cyanide, studies conducted on cyanide-free baths. In addition, cyanide strike silver baths added to the literature to increase the adhesion strength between the substrate and the coating. With these baths, it is aimed to improve adhesion and make a thin coating; silver cyanide baths are preferred to increase the coating thickness [49].

2.2 Electroless Plating: Overview

In electroless deposition a liquid electrolyte is used to reduce metal ions during electroless plating [61]. In 1835, Von Liebig described electroless deposition using aldehydes to reduce Ag(I) salts to Ag metal [62]. Electroless coating research started with the use of sodium hypophosphite as a reducing agent for the production of nickel coating and observed in the laboratory by Wurtz in 1844. However, he only obtained a black powder and that is the study of the beginning of the development of electroless deposition [63]. The first metallic Ni-P coating was carried out by Breteau in 1911 [64], followed by Roux in 1916 where the first patent for electroless nickel plating was obtained [65]. Although more research has been done with the developing technology and time, the process was developed more than 100 years later by A. Brenner and G.E. Riddell [66], who developed an acid electroless nickel plating formulation (Figure 2.2). Electroless copper chemistry was first reported the following year by Narcus [67].

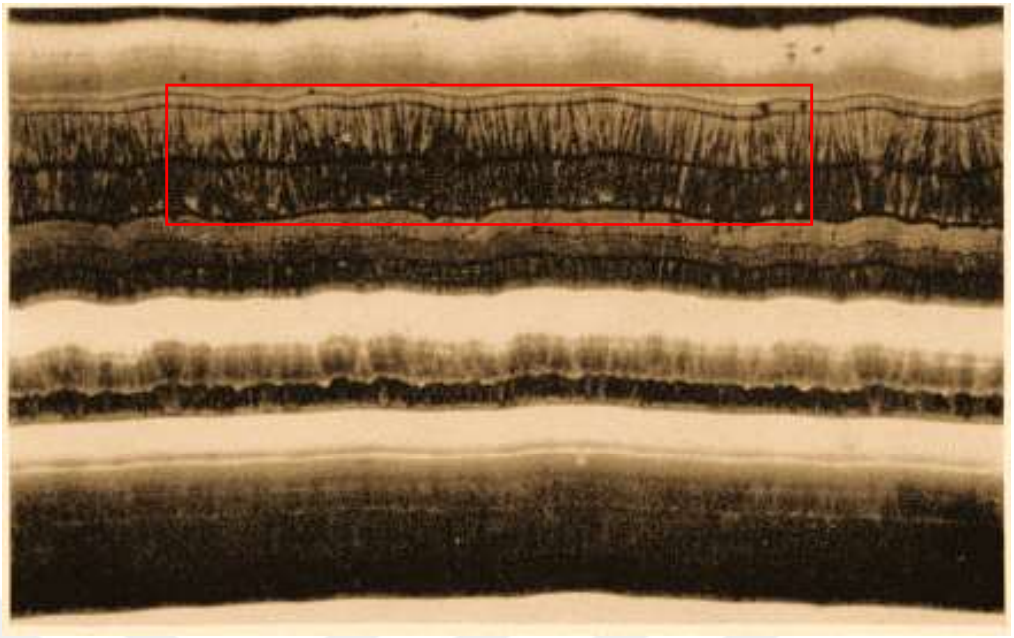

Figure 2.2 Electroless columnar nickel deposition from acidic solution. Reproduced from [66].

Brenner and Riddell described an autocatalytic process of depositing metal in the absence of electricity. Due to the fact that other metal depositions from aqueous solutions are carried out without the use of an external current, this process can be divided into three main groups; (i) Displacement Deposition, (ii) Contact Deposition, (iii) Autocatalytic Deposition [62].

i) The displacement deposition is a process which is include reducing noble metal ions and depositing them on the surface of an active metal due to its dissolution. Typical cementation systems in practice can be exampled as Cu/Al [68], Ag/Zn [69], Ag/Cu [70], Cu/Zn[71], Cu/Fe [72,73]. In displacement mechanism, reaction stops instantly when covers the surface. For this reason, deposition thickness is limited by reaction. In many cases, the adhesion of deposited films is inferior to that of electrodeposited or auto-catalytically deposited films. However, it differs from autocatalytic deposition in absence of a reducing agent [74]. When substrate is immersed in solution, the reactions can be explained scientifically by electrochemical series in Table 2.2. It can be examined with Cu/Fe system. The more electropositive redox system, copper (E = + 0.337 V), will be reduced while more electronegative,

iron (E = - 0.44), will undergo oxidation [45]. The anodic side reaction as $Fe \rightarrow Fe^{2+}$ while the cathodic side reaction of $Cu^{2+} \rightarrow Cu$ takes place.

Table 2.2 Standard electrode potentials of metals at 25°C. Reproduced from [45].

pH	Equilibrium	Normal hydrogen scale (V)
0	$Ag^{+} + e^{-} \rightarrow Ag$	+ 0.799
	$Cu^{2+} + 2e^{-} \rightarrow Cu$	+ 0.377
	$HCOOH + 2H^{+} + 2e^{-} \rightarrow HCHO + H_2O$	+ 0.056
	$Ni^{2+} + 2e^{-} \rightarrow Ni$	- 0.250
	$Fe^{2+} + 2e^{-} \rightarrow Fe$	- 0.440
	$H_2PO_3^{-} + 2H^{+} + 2e^{-} \rightarrow H_2PO_2 + H_2O$	- 0.50
	$Zn^{2+} + 2e^{-} \rightarrow Zn$	- 0.763
14	$HCOO^{-} + 2\ H_2O + 2e^{-} \rightarrow HCHO + 3OH^{-}$	- 1.07

ii) In contact deposition, there is a small equivalent to electroplating without need any external electrical source. A galvanic element supplies the required flow of electrons and it contains metal which deposition takes place (cathode) and auxiliary metal (anode). The anode dissolves and deposition takes place on cathode surface [62]. Contact deposition is not widely used method for electroless plating, generally this process preferred in electroless nickel plating on Cu/Cu Alloys. Another example of contact deposition is copper-potassium and silver cyanide system. In this system, silver ions generate an electrical current and reduce on the copper sheet. To yield good results, contact deposition electrolytes must possess definite properties: it must have good conductivity, as the current generation is weak, and they must also attack the metal chemically [75].

iii) Autocatalytic deposition is a chemical method for deposition of metallic coatings from aqueous solutions. In mechanism of autocatalytic deposition, metallic coating forms on catalytically active surfaces without need of external electricity. Reducing agent provides chemical reduction of metal ions in aqueous solution. Reaction between metal ion and reducing agent is shown in Equation (2.1) [62].

$$M^{z+} + R^{n-} = M + R^{z-n} \quad \textbf{(2.1)}$$

In order to form coatings except for systems with thickness limitation (***i.displacement deposition***) (Figure 2.3), an oxidation reaction can take place other than the dissolution of the substrate and metal. With the chosen reducing agent, more negatively than the metal to be coated, electrochemical reactions occur only as accumulation on the substrate. For example, formaldehyde (E = + 0.056), used as a reducing agent used in electroless silver plating baths, reacts with silver nitrate (Ag^{+}/Ag, E = + 0.799), which is a source of silver [45]. Various aluminum parts that are not suitable for electroplating are chemically plated with nickel in the aircraft industry for a variety of applications. However, electroless plating is too expensive to be used when conventional electroplating can be used [76].

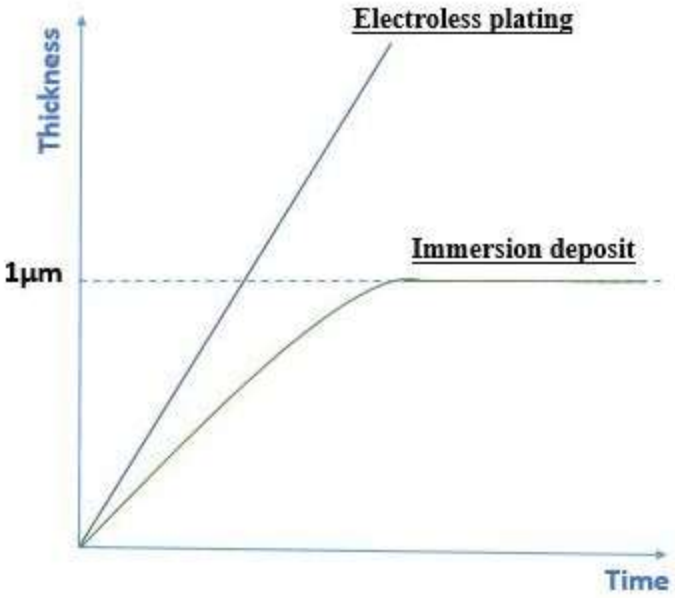

Figure 2.3 Plating thickness vs time relation for deposit and electroless plating. Reproduced from [45].

Electroless plating offers several advantages over electrochemical deposition. The first of these is the availability of coating on complex structures. Secondly, thin metal film formation on nonconductive surfaces (i.e., glass, ceramic, polymer, etc.) is also

possible with electroless coating. It has a very simple system and provides a very homogeneous coating thickness on all activated surfaces. In corrosion and electronics applications, electroless deposition deposits possess better properties because they are dense (no pitting) [62]. However, it also need to consider the information that the chemicals used in plating solutions can be hazardous just like in electroplating, and appropriate methods should be determined for the disposal of these chemicals. For example, cyanide and thiourea usage are the problems for electroless gold plating and nickel plating baths [77].

The deposition of metals and/or alloyed metal coatings with electroless methods has been preferred for applications such as electronics [79,80], medical devices [81,82], and battery technologies [82], along with advanced technology. When suitable bath composition and suitable conditions are provided (pH, temperature, time, catalyzed surface with activation, etc.), metal deposition is performed on metal or non-metal substrates.

2.3 Deposition Mechanism of Electroless Plating Baths

Unlike electroplating, there is no need for an external current source as the reducing agent in the bath composition provides the electron source for the reduction. Therefore, simple beaker chemistry is sufficient. Almost any surface can be coated, even those that require chemical modification by catalyzing the surface with suitable catalyst particles (Sn, Pt, Pd, Ag, etc.) [83]. The reduction of the metal from the aqueous solution takes place thanks to the reducing agent dissolved in the electroless bath. It provides the attachment of reduced ions on activated surfaces (for nonconductive substrates) or on surfaces that do not require metallization (for metals or conductive substrates) [84]. In electrode reactions, H^+ or OH^- ions are often involved, and the electrode potential is affected by their concentration (or pH of the solution). As a result of the dissociation equilibrium of water, these ions have interrelated activities as:

$$a_{H^+} + a_{OH^-} = K_W = 1.27 \times 10^{-14}\ mol^2/L^2 \qquad \textbf{(2.2)}$$

Because of this reason, reactions can be formulated as for acidic solution:

$$2H^+ + 2e^- \rightleftharpoons H_2 \quad \textbf{(2.3)}$$

For alkaline solution:

$$2H_2O + 2e^- \rightleftharpoons H_2 + 2OH^- \quad \textbf{(2.4)}$$

According to thermodynamics, two ways are equivalent and Equation (2.3) and Equation (2.4) can be written in two ways. However, E^0 values are differ, because sometimes $a_{OH^-} = 1$ in the other $a_{H^+} = 1$. On the scale of the standard hydrogen electrode (SHE), standard potential of acidic solution ($E_A^0 = 0$) equal to zero. According to Equation (2.4), a_{OH^-} nearly equal to 1, so $E_B^0 = -0.822$ V. Changes in reactants and (or) products with solution pH will affect the values of E^0 and pH dependence of electrode potential. As a result, phase diagrams constructed in the coordinates of E and pH clearly illustrate these changes. These diagrams were suggested by Marcel Pourbaix in 1963 and became known as Pourbaix diagrams. In Figure 2.1, an example of Pourbaix diagram for Ag electrode at room temperature and pH range is 0 to 14. Solid lines delimit the thermodynamic stability regions of specific compounds in the diagram. This stability is relative. The diagram's dashed line represents the hydrogen electrode's equilibrium potential. It is possible to oxidize metallic silver when the reaction lines are located below the hydrogen electrode line [85].

In order to understand the reduction behavior in electroless plating baths, metal-water and reducing agent-water potential-pH diagrams should be examined. In order for the reducing of metal, it is necessary to go below the region where the metal is stable according to the Pourbaix diagram. For example, when the Ni-Water potential-pH diagram (Figure 2.4) examined, nickel ions are more stable over - 0.25V at acidic pH; it is observed that solid nickel metal is more stable under - 0.25V. The following reactions occur when sodium hypophosphite, which is used as a reducing agent, is oxidized under - 0.25 V [45]:

$$\textbf{Cathode: } Ni^{2+} + 2e^- \rightarrow Ni \qquad E = -0.25 \text{ V} \quad \textbf{(2.5)}$$

Anode: $H_2PO_2^- + H_2O \rightarrow H_2PO_3^- + 2H^+ + 2e^-$ $E = -0.50$ V **(2.6)**

In addition, the potential of formaldehyde that used as a reducing agent in electroless copper plating baths varies in acidic and basic environments. For example, when pH=0, the potential value is 0.056 V; the potential value (pH=14) in alkaline environments was recorded as - 1.07 V [45]. Therefore, this data shows that in the use of formaldehyde as a reducing agent, it is preferred in basic baths. When these conditions are met, anodic/cathodic reactions occur when a suitable substrate immersed in a plating bath.

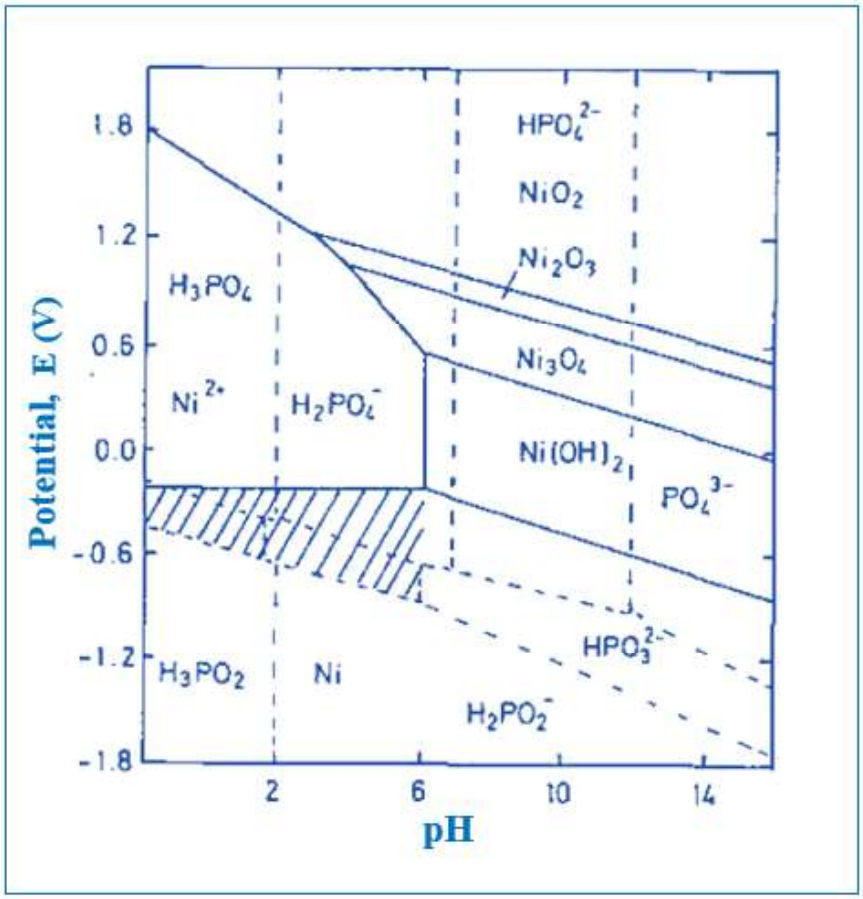

Figure 2.4 The combined potential pH diagram for the nickel water and phosphorus water system. Reproduced from [45].

2.4 Electroless Silver Plating

In 1835, an aware of the toxic effects of mercury used in mirror making, Justus von Liebig proposed that aldehydes reduced silver salts to metallic silver (Ag (I) to Ag^0). Copper and ammoniacal silver nitrate were combined with sugar by Liebig to create flawless mirrors [86].

Despite their efficiency and associated hazard of forming the dangerously explosive fulminating silver, Brashear, cane sugar, Rochelle salt, and formaldehyde processes are no longer widely favored for reducing silver. It was deliberately avoided to add too much ammonium hydroxide to these solutions of silver ammonium-nitrate [87]. However, with the developing technology, reducing agents added to the system in order to prevent the dangers that may occur in the presence of excessive ammonia and they eliminate the formation of fulminating silver. For example, when hydrazine hydrate is included in the silver-ammonium nitrate complex (product of Equation (2.13)), the reduction reaction of silver (Equation (2.10)) and silver metal deposition takes place on catalytically active surfaces. In Table 2.3 cyanide-free electroless silver plating bath compositions, operation parameters and thickness information obtained at the end of the specified time are shared. Baths containing cyanide are shared in Appendix B.

Table 2.3 Electroless silver plating baths with $AgNO_3$ non-cyanide baths.

No	Silver Source	Reducing Agent	Complexing Agent	Stabilizer	Temp. (°C)	pH	Duration (hr)	Plating Rate (μm/hr)	Ref.
1	$AgNO_3$	$N_2H_4.H_2O$	NH_4OH	$(NH4)_2CO_3$	83	8.0-13.0	1	2	[88]
	1.67 g/L	0.35 g/L	200 mL/L	70 g/L					
2	$AgNO_3$	$N_2H_4.H_2O$	NH_4OH	$(NH4)_2CO_3$	81	8.0-13.0	0.5	2	[88]
	1.67 g/L	0.30 g/L	150 mL/L	150 g/L					
3	$AgNO_3$	$N_2H_4.H_2O$	NH_4OH	$(NH4)_2CO_3$	80	8.0-13.0	1	1	[88]
	1.67 g/L	0.4 g/L	350 mL/L	150 g/L					
4	$AgNO_3$	$N_2H_4.H_2O$	NH_4OH	$(NH4)_2CO_3$	77-90	8.0-13.0	0.5	1.4-1.6	[88]
	1.67 g/L	0.3 g/L	300 mL/L	150 g/L					
5	$AgNO_3$	$N_2H_4.H_2O$	NH_4OH	$(NH4)_2CO_3$	60-65	8.0-13.0	0.33	0.6-1.2	[88]
	0.835	0.2 g/L	250 mL/L	150 g/L					

Table 2.3 Electroless silver plating baths with AgNO3 non-cyanide baths.

6	$AgNO_3$	Seignette salt	Na_2EDTA-Ethylene diamine	Dipy/ Bhpy	60	12.0	1	6.2	[89]
	3.4 g/L	16.7 g/L	16.7 g/L-22.5 g/L	--/--					
7	$AgNO_3$	Seignette salt	Na_2EDTA-Ethylene diamine	Dipy/ Bhpy	55	12.5	1	5.7	[89]
	3.4 g/L	16.7 g/L	16.7 g/L-22.5 g/L	-- /0.001g/L					
8	$AgNO_3$	Seignette salt	Na_2EDTA-Ethylene diamine	Dipy/ Bhpy	--	--	1	3.9	[89]
	3.4 g/L	16.7 g/L	16.7 g/L-22.5 g/L	0.0005g/L/ 0.001g/L					

Table 2.3 Electroless silver plating baths with AgNO3 non-cyanide baths.

9	$AgNO_3$	Seignette salt	Na_2EDTA-Ethylene diamine	Dipy/ Bhpy	--	--	1	3.8	[89]
	3.4 g/L	16.7 g/L	16.7 g/L-22.5 g/L	0.001g/L/ 0.001g/L					
10	$AgNO_3$	CH_2O	NH_3-$Na_3C_6H_5O_7$	Invertose	RT	>8.0	0.08	1.44	[90]
	0.015 g/L	0.001 mL/L	0.05 g/L-0.05g/L	0.05 g/L					
11	$AgNO_3$	NH_3	$Na_3C_6H_5O_7$	--	15	>8.0	0.025	1.4	[90]
	0.01 g/L	0.05 g/L	0.08 g/L	--					
12	$AgNO_3$	$N_2H_4.H_2O$	--	NH_3-NaOH	--	8.5	0.16	-	[90]
	0.05 g/L	0.02 g/L	--	--					
13	$AgNO_3$	$N_2H_6SO_4$	--	$C_2H_3NaO_2$ .NH_3	--	9.0	0.08	-	[90]
	0.01 g/L	0.01 mL/L	--	0.05- --					

Table 2.3 Electroless silver plating baths with AgNO3 non-cyanide baths.

14	$AgNO_3$	$C_6H_{10}O_6$	NH_3	NaOH	25	12.0	--	--	[91]
	5 g/L	2.25 g/L	9.5 mL/L	5 g/L					
15	$AgNO_3$	CH_2O	NH_4OH	SLES-CH_3COOH	65	9.0	2	--	[92]
	52.86 g/L	33.1 mL/L	22.88mL/L 2.17M	25.49 mL/L-10 mL/L					
16	$AgNO_3$	$C_6H_{10}O_6$	NH_3	CH_3COOH	--	10.2	0.008	$5.1x10^{-7}$	[93]
	0.0032 mol/L	0.01 mol/L	2.24 mol/L	0.56 mol/L					
17	$AgNO_3$	$C_6H_{12}O_6$-$C_4H_6O_6$-C_2H_6O	NH_3	CH_3COOH	50	--	0.5	--	[94]
	7.5 g/L	40g/L-1g/L-100mL/L	10 mL/L	--					

2.5 Metallization Procedure for Electroless Silver Plating

In autocatalytic metal plating, non-electrolytic deposition from solution is carried out. The thermodynamically unstable solution becomes stable with a suitable catalyzed surface. After the coating is initiated on the catalyzed surface, the coating reaction is driven by the catalytic nature of the coated metal surface. This definition of electroless coating thus covers both solutions that have a homogeneous chemical reduction on all surfaces, such as silver mirroring solutions, and dip-coating solutions that deposit a very thin film on a relatively noble metal by displacement on the surface [95].

Surface refinement of metallic films by chemical reduction requires the cleanliness of the substrate. Deposition rate and thickness can be affected by the sensitization procedure, which improves the uniformity and adhesion of the precipitate. In most cases, activators and catalysts contain some precious metal, such as palladium, platinum, or gold.

Pretreatments are necessary for coating processes on catalytically inactive materials, such as degreasing, etching, sensitizing with Sn^{2+} ions, and activating by reducing Pd^{2+} ions. Sensitizers for silver reduction have been shown to include tin salt. It has been reported by O. Macchia [96], immersion in a dilute solution of stannous chloride for 10 seconds greatly facilitates the formation of silver mirror and its adhesion to glass. Hydrolysis of the stannous chloride result in a formation of gelatinous film of stannous hydroxide, which is very adherent to glass, cellulose, and wood plates.

The two-step metallization process ($SnCl_2$ sensitization and $PdCl_2$ activation) was described by Bergström in a report published in 1950 [97]. Sensitizers for silver reduction have been shown to include tin salt [96]. Adsorption of the stannous ion (Sn^{2+}), sensitization, was performed in step 1 using stannous chloride and hydrochloric acid solution. Sn^{2+} formed by the hydrolysis of SnO_2 in the sensitization solution adheres to the sample surface, so the positively charged fine silver ions are reduced by Sn^{2+} then attach to the surface. Then activated surface immersed in the electroless coating bath. Even when the bath is not in use, the tin ions should be checked regularly and the sensitization bath should be rebuilt if it is necessary. Because the stannic ion

passes into the stable phase (Sn^{4+}) and this causes the bath to be out of use because it cannot reduce the palladium [98].

A thorough rinse was then performed on the part. A palladium chloride/hydrochloric acid solution was used in step 2 to reduce the Pd^{2+} ion to Pd^{0} when immersed in it with the stannous ion with respect to Equation (2.7) [98]. Nucleation zones are formed on the surface of the ceramic with the activation process, thus making it easier for the coating to adhere to the surface. During the activation process, mechanical attachment to metal or dielectric surfaces occurs. Activation solutions usually contain palladium reduced by tin ions and have high chloride ions and acidity. The number of tin atoms is 50 to 100 times greater than palladium and smaller in size (Figure 2.5) [99].

$$Sn^{2+} + Pd^{2+} \rightarrow Sn^{4+} + Pd^{0} \quad \textbf{(2.7)}$$

Figure 2.5 shows the schematic illustration of Pd formation from $PdCl_2$ salt and according to the Equation (2.7). To produce catalytic sites with diameters of 10 Å, two-step metallization process applied [100]. For the metallization process, surface morphology and surface roughness are important parameters. Based on the results of real experiments, the sample surface after the metallization process facilitates the reduction of the metal coating to be applied. On selective and continuous surfaces of activated dielectric samples, electroless coatings deposited homogeneously.

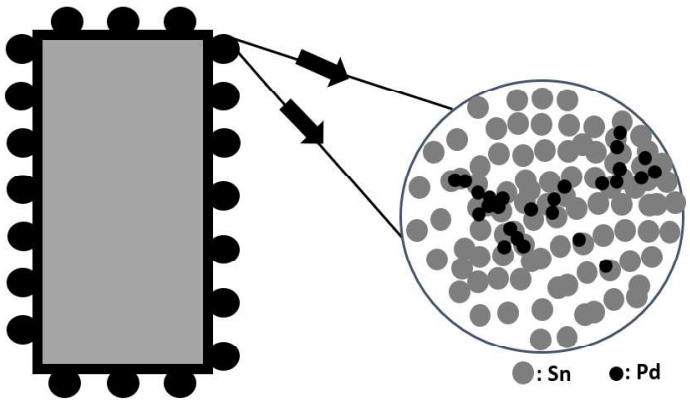

Figure 2.5 Activation mechanism between stannous chloride and palladium chloride salt. Reproduced from [99].

For acidic sensitization and activation solutions, the appropriate acidity level is defined as pH=1 to 5, and the most appropriate value is approximately pH=2.5. Appropriate concentration is about 1 to 10 weight percent $SnCl_2$; 0.5 to 1 is used as $PdCl_2$. Apart from the degree of acidity, the temperature and time also affects the quality of the coating to be obtained in the final [97]. During the palladium activation process, immersion for a long time should not be preferred. Lau et al examined palladium nucleation processes based on nucleus size distribution on TiN (Figure 2.6) [101]. Observations obtained within the 1-minute activation time showed that the particle distribution was narrower and 30 nm. When the time increased to 2 minutes, the particle size distribution increased and the information that the particle sizes were 60 nm had been obtained. When the activation time was extended to 3 minutes, it was observed that the size of the Pd nucleus decreased (nearly 50 nm), the distribution narrowed, and the secondary nucleation increased.

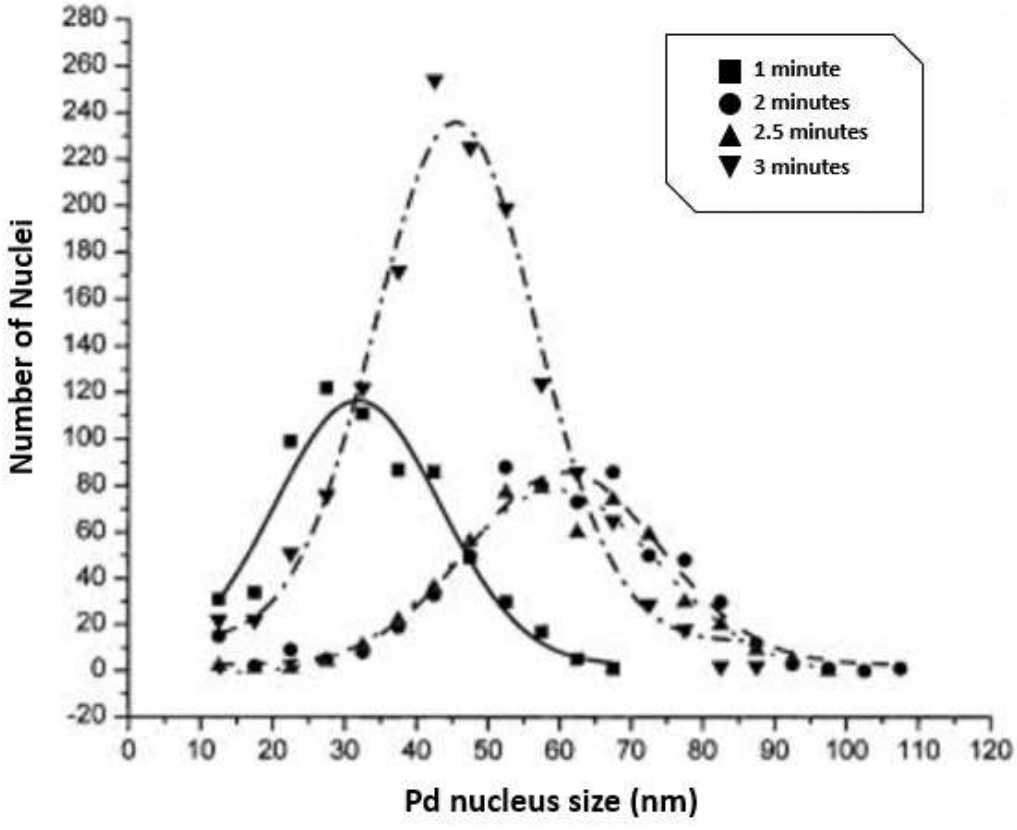

Figure 2.6 Number of nuclei vs nucleus size for Pd with respect to time. Reproduced from [101].

Apart from the 2-step method, that used as the metallization of non-conductive materials and has a high success rate due to the strong adhesion of tin ions to the surface [102]. It also includes different options; i) Acidic solutions of divalent metal salts (e.g. $PdCl_2$ or $PtCl_2$) can use for the one-step metallization process [103], ii) The palladium-tin colloid system [104], [105], [106], [107] (approximately 1-5 nm in size) is the more preferred method commercially, which contains a palladium-rich inner core and Sn (IV) chloride in the outer sphere. Excess Sn (II) is important in terms of solution stabilization, and its more stable structure provides an advantage over others, iii) Copper catalyst, first reported in 1976 [108] and then 1979 [109], was preferred over palladium for cost reduction. However, it has proven to be inefficient as it is less catalytically active, iv) the ionic complex palladium system was developed in the mid-1970s [120,121], but in order to be catalytically active, it is activated with the support of a reducing agent such as DMAB [112].

2.6 Baths for Electroless Silver Deposition

Typically, the constituents of a solution for electroless metal deposition are (i) Source/Sources of metal ions, (ii) Reducing agent(s), (iii) Complexing agent(s), and (iv) Stabilizer(s) and inhibitor(s) [62].

2.6.1 Metal Ion Sources

Nitrates, sulfates, chlorides, acetates, cyanides, etc., are water-soluble salts that can contain metal ions. A general metal ion source for specified metals are shown in Table 2.4. In general, the metal ion source determined by the stability of the solution, the properties of the deposited films, and the environment.

Table 2.4 Common metal sources of specific metals. Reproduced from [62].

Metal	Source of Metal
Ni [62]	$NiSO_4$, $NiCl_2$, $Ni(H_2PO_2)_2$, $Ni(CH_3COO)_2$
Cu [113]	$CuSO_4$, $CuCl_2$, $Cu(NO_3)_2$
Co [62]	$CoSO_4$,$CoCl_2$
Ag [62]	$AgNO_3$, $NaAg(CN)_2$
Pd [62]	PdCl, $Pd(NH_3)_4Cl_2$

2.6.1.1 Silver Nitrate

Silver is preferred because of its high conductivity, corrosion, and wear properties as mentioned in section 2.1. Silver nitrate, a silver salt, chosen in electroless silver-plating baths, also includes an environmentalist approach in terms of not containing a harmful composition, unlike the toxic components of silver cyanide. Silver nitrate reacts initially with the complexing agents and then with the reducing agent in the electroless silver-plating bath [88]. When silver nitrate is treated with ammonium hydroxide Equation (2.8) [64]), Ag_2O is formed as the first product, followed by $[Ag(NH_3)_2]NO_3$ and ammonium hydroxide Equation (2.9) [64]). Because of the reaction between the reducing agent and the silver complex, Ag^0 obtained.

$$2AgNO_3 + 2NH_4OH = 2\ Ag^+ + O^{2-} + 2NH_4NO_3 + H_2O \quad \textbf{(2.8)}$$

$$[Ag(NH_3)_2]OH + 4\ NH_4NO_3 \rightleftharpoons [Ag(NH_3)_2]NO_3 + NH_4OH \quad \textbf{(2.9)}$$

2.6.2. Reducing Agents

The choice of reducing agent depends on the metal or alloy desired to be deposited, as well as on the plating bath conditions and physico-chemical properties [62]. Table 2.5 shows commonly used reducing agents and complexing agents for the specific pure metal deposition process. Formaldehyde and hydrazine hydrate generally preferred in baths established for the purpose of pure metal deposition.

Table 2.5 Common reducing agents used in electroless plating bath. Reproduced from [45].

Deposited Metal	Common Reducing Agents	Common Complexing Agent	Substrates
Ni	Sodium hypophosphite Sodium borohydride Hydrazine Dimethyl amine borane	Citric Acid Oxalic Acid Tartaric Acid EDTA	Ni, Co, Fe, Pd, Rh

Table 2.5 (continued) Common reducing agents used in electroless plating bath. Reproduced from [45].

Co	Sodium hypophosphite Sodium borohydride Hydrazine Dimethyl amine borane	Citric Acid Oxalic Acid Tartaric Acid EDTA	Ni, Co, Fe, Pd
Cu	Formaldehyde Dimethyl amine borane	Sodium potassium tartrate EDTA Glycolic Acid Triethanol amine	Cu, Au, Ag, Pt, Pd
Ag	Formaldehyde Hydrazine hydrate	EDTA Ammonium hydroxide	Cu, Brass, Au, Ni
Pd	Sodium hypophosphite Hydrazine	EDTA Ammonia	Co, Au, Fe, Ag, Ni

2.6.2.1 Hydrazine Hydrate

Hydrazine hydrate is a powerful compound that generally used in deposition of pure metal in aqueous plating baths. It also preferred in spray method for silver mirror production because of its high deposition rate [114].

Hydrazine hydrate is preferred in electroless silver plating baths containing silver-ammonia compound. The use of hydrazine hydrate as a reducing agent in baths containing silver-ammonia complex is preferred because of the high coating speed it provides, conductivity value, and the same time to form complex with high stability (Table 2.6). Equation (2.10) [62] is realized with the addition of hydrazine hydrate to the bath. The summary reaction between the silver-ammonia complex and hydrazine is given in Equation (2.11) [114]. Silver cations are reduced to metallic state by reaction of hydrazine hydrate.

$$4Ag(NH_3)_2^+ + N_2H_4 = 4NH_4^+ + 4NH_3 + N_2 + 4Ag \quad \textbf{(2.10)}$$

$$4Ag^+ + N_2H_4 + 4\ OH^- = 4Ag + N_2 + 4H_2O \quad \textbf{(2.11)}$$

Table 2.6 Electroless silver plating with hydrazine plating rate and resistivity with respect to EDTA and ammonia complex. Reproduced from [114].

Agent	**Plating Rate (μm/min)**	**(μohm-cm)**	
		22°C	120°C
EDTA	0.9	7	3-5
NH_3	1.9	2.8	1.9

The potential of hydrazine shown in Figure 2.7 that used as a reducing agent in electroless silver plating baths, varies in acidic and basic environments. According to graph, decreasing in hydrazine concentration the potential of hydrazine increase but at the same time pH of the solution decrease. The minimum potential (E= - 4.0 V) obtained at high alkalinity (pH=10.5) and high concentration of hydrazine. As a result, this data suggest that hydrazine is preferred to be used as a reducing agent in basic baths for silver (E= + 0.799) suitable substrate immersed in a plating bath will undergo anodic/cathodic reactions when these conditions are met.

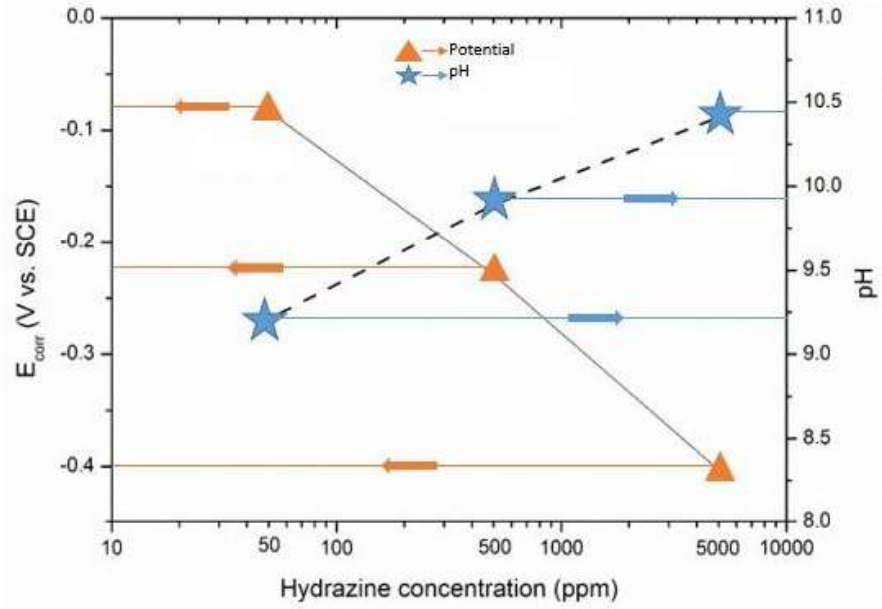

Figure 2.7 Change of E and pH of hydrazine with respect to concentration. Reproduced from [115].

2.6.3 Complexing Agents

Only metal salt and reducing agent do not guarantee successful results in electroless coating baths. By-products that may occur because of the reaction of the reducing agent with metal ions and reduce the yield. In this context, complexing agents add to electroless coating baths to prevent by-products that may occur. Thus, the free metal ion concentration is kept below the saturation level of the bath and at the same time, the working pH is balanced [45].

2.6.3.1 Ammonium Hydroxide

The generally preferred complexing agent is ammonium hydroxide NH_4OH [88,91-93]. The use of 28% ammonium hydroxide in electroless silver plating baths causes pH rise by dissolving into NH_4^+ and OH^- ions as given in Equation (2.12) after dissolving in water. When the working pH range (8-11) of electroless silver baths is examined, the use of ammonium hydroxide would be the right choice. At the same time, the silver salt, which is frequently preferred in electroless silver plating baths, forms $Ag(NH_3)_2$ as a result of its reaction with $AgNO_3$ Equation (2.13) and is a species ready to react with this complex hydrazine hydrate.

$$NH_4OH \rightarrow NH_4^+ + OH^- \quad \textbf{(2.12)}$$

$$AgNO_3 + NH_4OH \rightarrow [Ag(NH_3)_2]NO_3 + 2H_2O \quad \textbf{(2.13)}$$

2.6.4 Stabilizers/Controlling Agents

Stabilizers that defined as chemical compounds used to stabilize undesirable formations in the bath and prevent the deterioration of the bath. To exemplify such agents, generally preferred in low concentrations in the bath, it can classify as mercaptobenzothiazole, thiourea, other sulfur compounds, cyanide or ferrocyanide salts, mercury compounds, molybdenum and tungsten, heterocyclic nitrogen compounds, methyl butanol, propionitrile and the like [103]. The addition of compounds to the bath composition guarantees a long bath life when suitable concentration, pH, and temperature conditions are provided [117].

Control agents optimize parameters such as coating speed, stability against metal oxide formation, and high bath activity. Spontaneous decomposition of the bath (triggering), decomposition over a prolonged standing period (plate-out), inability to induce a controlled plating reaction when first stored after makeup (second-day startup), dark deposit color, rough deposit, coarse grain structure can be prevented by controlled additions. Among the materials evaluated under the title of speed promoter, compositions such as ammonium carbonate, nitrates, chlorides, chlorates are around 0.1 M in electroless coating baths [118].

2.6.4.1 Ammonium Carbonate

Electroless silver plating baths are generally very unstable and there are many types of stabilizers used in deposition of silver. They include metal ions of copper, nickel, cobalt, zinc and gold [119], tetrabutylammonium nitrate and dodecylammonium acetate [120], ammonium carbonate [88], and ethylene diamine [116]. Three iodotyrosine or three-five diiodotyrosine significantly increased the stability of electroless Ag deposition solutions (pH 10 to 10.5) [117]. It is generally preferred to use either ammonium carbonate ($(NH_4)_2CO_3$) and/or ammonium bicarbonate

(NH_4HCO_3) as a stabilizer for electroless silver plating. An optimal amount of ammonium carbonate and/or bicarbonate ranges from 0.01 to 360 grams per liter, more preferably 10 to 200 grams per liter [88].

2.6.5 Chelating Agents

In order to obtain a sufficient number of free metal ions for deposition, the concentration and selection of the complexing agent must be carefully considered. In general, ethylenediaminetetraacetic acid (EDTA) used for the electroless deposition of metals. For plating to continue, it requires very careful control due to its high stability constant [45].

2.6.5.1 Ethylenediaminetetraacetic acid disodium salt dihydrate (EDTA disodium salt dihydrate)

EDTA disodium salt dihydrate is also widely used as a complexing agent in electroless plating baths. Due to its high affinity in electroless baths, EDTA can attract potentially toxic metals or unwanted complex formations into the waste stream, even in small quantities. The use of EDTA as a chelator in baths has attracted a lot of attention in countries such as Germany and Japan and has led to it being preferred in common bath ingredients [118].

CHAPTER 3

EXPERIMENTAL PROCEDURE

First, the ceramic composition, selected after the literature review within the scope of determining the base ceramic composition, was produced by tape casting for coupon-based production. At the same time, the plating bath content was determined for the electroless silver plating process. Roughening, alkaline acid cleaning, 2-step and different metallization processes were carried out on CT-CZN x32 ceramics produced by tape casting. Coating thickness and bath stabilization at different temperatures were investigated. In addition, in order to observe the chelating agent effect, EDTA was prepared in fixed molarity and was added in specific amounts to the electroless coating bath and its effect was examined. XRF, OM, and SEM analysis for determination of coating thickness; XRD and XRF analyzes for composition determination were performed on the sample after electroless silver plating. Also, 4 point prop resistivity measurements were performed to obtain conductivity value of silver plating.

3.1 Production of Ceramics

Figure 3.1 includes the flow chart of ceramic processing and characterization steps. The ceramic production process begins with the preparation of the starting powders (Section 3.1.1). The casting solution prepared for tape casting poured using a 250 μm blade. After drying, samples were cut into 2x2 cm^2 dimensions, and then placed on top of each other in 15 layers. To increase adhesion, they were kept in an oven at 80°C for 20 minutes and pressed for 5 minutes at 20 MPa. Samples were shaped and burnout process was carried out. Burnout and sintering profiles are shared in Figure 3.4 and Figure 3.5, respectively. In order to examine the phase formations, XRD analyses were performed and initial composition values were recorded by XRF-EDS. In addition, profilometer (Mitutoyo SJ-400) measurements were made to record the initial roughness values.

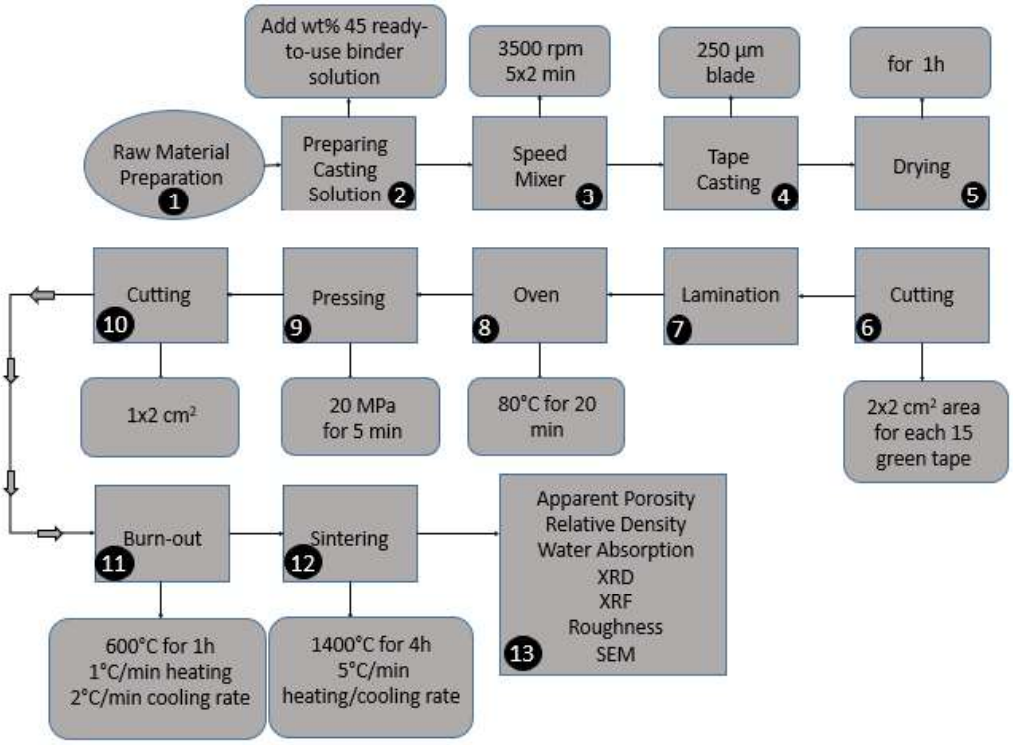

Figure 3.1 Flow chart of ceramic processing and characterization.

3.1.1 Raw Material Preparation

The starting powders required to form the CZN composition, CaO (99.9%, Nanography), ZnO(99.9%, Nanography), Nb_2O_5 (99.9%, Sigma Aldrich) were treated as shown in Figure 3.2. Then, phase formations were analyzed by X-Ray diffraction. Calcinated powders were mixed for 24 hours using 0.5 cm diameter yttria-stabilized zirconia balls according to the molar fraction 0.68CT-0.32Ca($Zn_{1/3}Nb_{2/3}$)O_3 in a ball mill with 2-4% binder. Then, the drying process was completed in magnetic stirrer at 250 rpm at 100°C, followed by oven drying at 40°C.

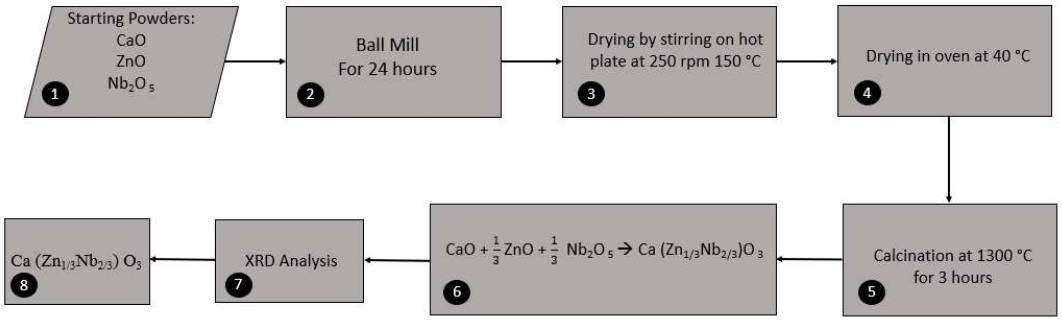

Figure 3.2 Process chart for $Ca(Zn_{1/3}Nb_{2/3})O_3$ (CZN).

3.1.2 Sample Preparation Processes

Powders prepared using a ball mill sieved through an 80 μm sieve to separate bigger particles. A solution of 55% 0.68CT-0.32CZN and 45% commercial tape casting solution was prepared. The slurry prepared for tape-casting was mixed 2 times for 5 minutes at 3500 rpm with a speed mixer (Speed Mixer, DAC 150 FVZ).

The tape casting process started with the placement of the doctor blade assembly. Casting slurry poured on a carrier surface with a speed of 5 cm/sec (Figure 3.3). Drying takes place by evaporation of the solvent.

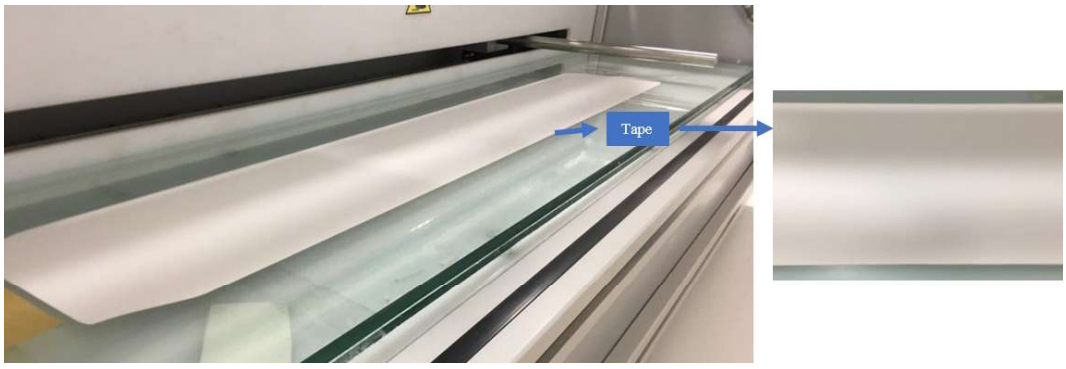

Figure 3.3 Drying process of green tape.

Finally, laminated green samples were cut into two pieces (1x2 cm) as seen in Figure 3.6a. Burnout carried out at 600°C for 1 hour, with a 1°C/min heating and 2°C/min cooling rate as shown in Figure 3.4.

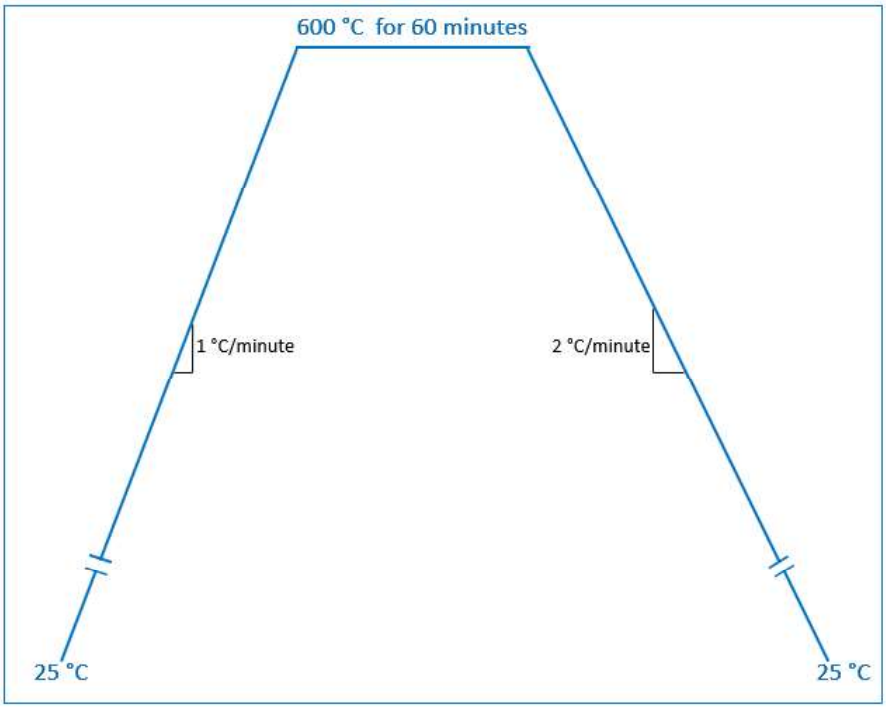

Figure 3.4 The temperature-time profile for burnout process.

Green samples were sintered at 1400°C for 4 hours in an alumina crucible with 5°C/min heating/cooling rate (Figure 3.5). Sintered samples and the preparation steps are shown in Figure 3.6. Green samples were placed in the crucible system (Figure 3.6b) in pairs and sintered. The wet, dry, and suspended weights of the sintered samples (Figure 3.6d) were measured.

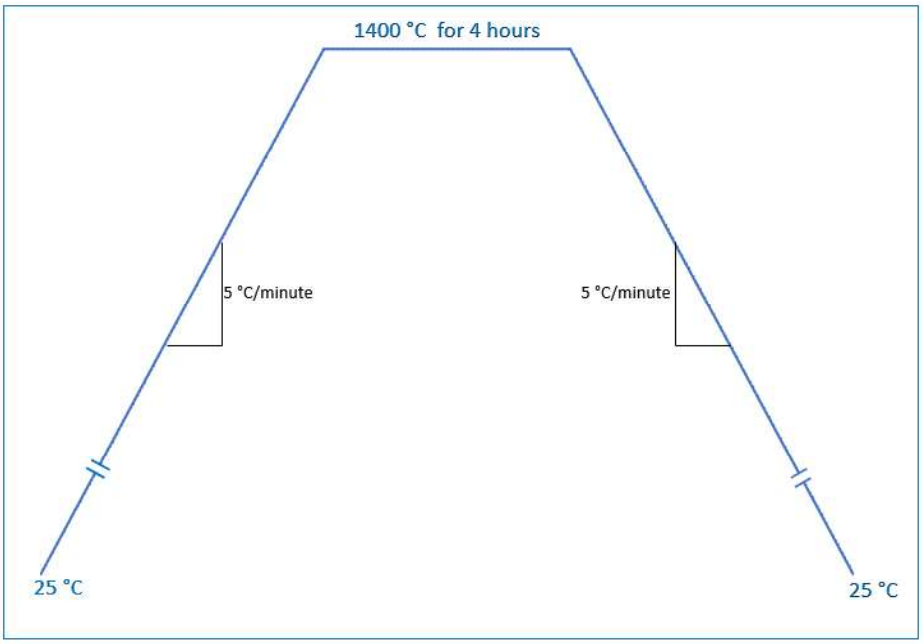

Figure 3.5 The temperature- time profile for sintering.

Figure 3.6 Sintering process of $0.68CaTiO_3$-$0.32Ca(Zn_{1/3}Nb_{2/3})O_3$ a) green bodies, b) green bodies on alumina crucible, c) crucible that placed on furnace, d) sintered ceramics on crucible, e) green tape (left) and sintered body (right).

Samples were kept in boiling distilled water at 100°C for 60 minutes and suspended, wet and dried weights were recorded. Densities were calculated using Equation (3.1) and Equation (3.2). Percent weight losses were determined by comparing dry weights of the samples before and after the sintering.

$$\rho_{bulk} = \left(\frac{Wd}{Ww - Ws}\right) \times \rho_{water} \quad \textbf{(3.1)}$$

$$\rho_{relative} = \left(\frac{\rho_{bulk}}{\rho_{relative}}\right) \times 100 \quad \textbf{(3.2)}$$

Phase formations of the sintered samples were obtained by Miniflex600, Rigaku X-ray diffractometer with CuKα radiation. XRD data was taken between 2θ = 10-80° with step size of 0.02° and a scanning speed of 2°C/minute.

Ceramic composition analysis were performed by Fischer Optiplex 3020 XDV XRF-EDS. The ceramic compositions were determined before and after the roughening processes and the changes were recorded.

3.2 Electroless Silver Plating

The electroless silver plating process includes pretreatment processes that precede it. These are etching, alkaline/acid cleaning, sensitization, and activation processes as shown in Figure 3.7. Within the scope of this study, grinding (180, 240, 320 Grid) and hydrofluoric acid (5 and 10 wt. %) etching were applied on the ceramic surfaces to increase the surface roughness. In order to remove the pollution and carbon/acid residues on the surface, alkaline and three different acid cleanings were carried out, and after the acid cleaning, the ceramic composition values were recorded by XRF. After the ceramic surface was metalized with sensitization and activation processes, it was immersed in the electroless silver plating bath.

Electroless silver plating solution composition contain $AgNO_3$ (1.57 g/L) as the silver source and hydrazine monohydrate (0.35 g/L) as the reducing agent. Preparing Solution-A bath start with dissolving of stabilizer $(NH_4)_2CO_3$ (70 g/L) and then complexing agent (NH_4OH 200 mL/L) in DI water. Mixed solution is heated to the plating temperature (45°C, 50°C, 55°C, 60°C, 70°C, 80°C) while specified reducing

agent is added to Solution A. As soon as the temperature reaches the desired point, dissolved silver nitrate in DI water (Solution B) is added into Solution A.

EDTA disodium salt ($C_{10}H_{18}N_2Na_2O_{10}$), used as a chelating agent for electroless silver plating bath at constant molarity (0.15 M) [43], was added to Bath 2 (B2) as 100 mL/L; to Bath 3 (B3) as 200 mL/L and plating rate in μm/hr was calculated at temperatures 50°C,60°C,70°C and 80°C. The operating parameters of B1, B2 and B3 and compositions of and chosen baths are shown in Table 3.1 and Table 3.2 respectively.

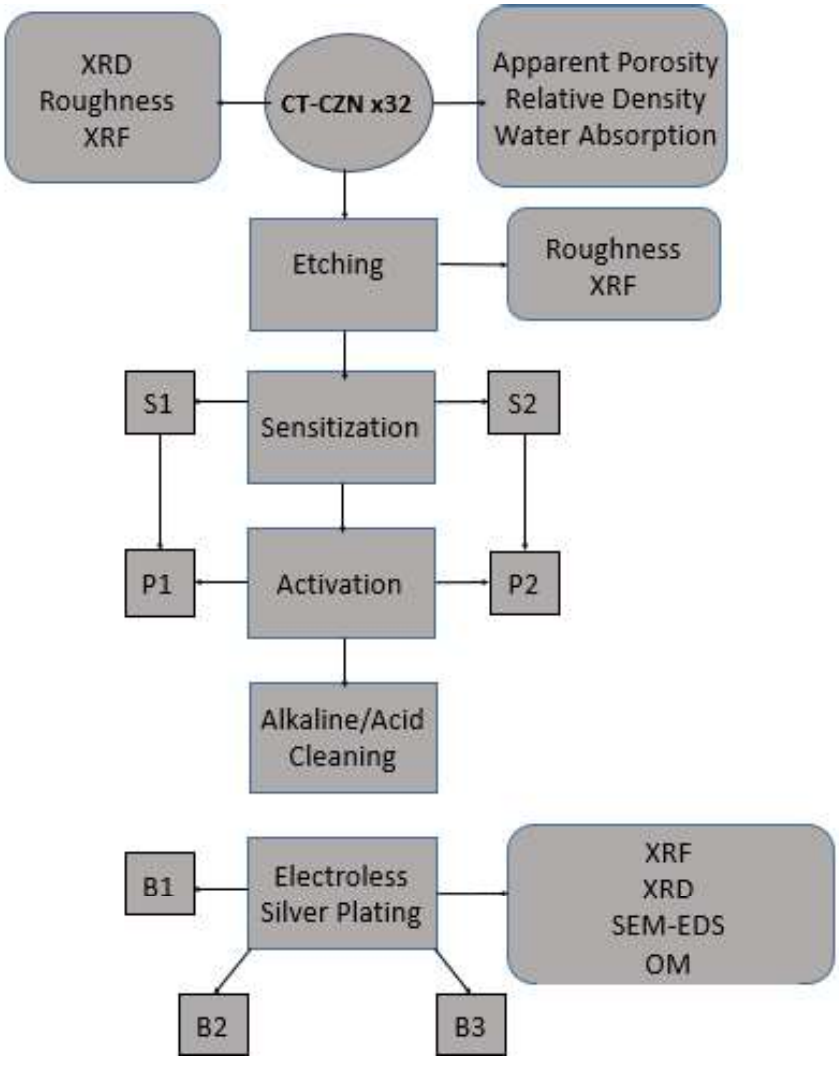

Figure 3.7 Flow chart for electroless silver plating on CT-CZN x32.

Table 3.1 Bath ingredients and parameter for experimental studies.

ID	Etching Type	Acid (2M)	Sensitization	Activation	Bath	Time (hr)	Temp. (°C)
CC5-2	-	H_2SO_4	-	-	-	-	-
CC5-3	-	HCl	-	-	-	-	-
CC5-4	-	H_3PO_4	-	-	-	-	-
CC5-5	-	H_3PO_4	S1	P1	B1	1	55
CC5-6	5% HF	H_3PO_4	S1	P1	B1	1	55
CC5-7	10% HF	H_3PO_4	S1	P1	B1	1	55
CC5-8	SiC-180	H_3PO_4	S1	P1	B1	1	55
CC5-9	SiC-240	H_3PO_4	S1	P1	B1	1	55
CC5-10	SiC-240	H_3PO_4	S2	P2	B1	1	55
CC5-11	SiC-320	H_3PO_4	S2	P2	B1	1	55
CC5-12	5% HF	H_3PO_4	S2	P2	B1	1	55
CC5-13	5% HF	H_3PO_4	-	P2	B1	1	55
CC5-14	5% HF	H_3PO_4	S2	P2	B1	1	60
CC5-15	5% HF	H_3PO_4	S2	P2	B1	1	50
CC5-16	5% HF	H_3PO_4	S2	P2	B3 $(G)^*$	1	80
CC5-17	5% HF	H_3PO_4	S2	P2	B3 $(PP)^*$	1	80
CC5-18	5% HF	H_3PO_4	S2	P2	B2	1	70
CC5-19	5% HF	H_3PO_4	S2	P2	B3	1	70
CC5-20	5% HF	H_3PO_4	S2	P2	B2	1	80
CC5-21	5% HF	H_3PO_4	S2	P2	B1	1	80
CC5-22	5% HF	H_3PO_4	S2	P2	B1	1	70
CC5-23	5% HF	H_3PO_4	S2	P2	B3	1	60
CC5-24	5% HF	H_3PO_4	S2	P2	B3	1	50
CC5-25	5% HF	H_3PO_4	S2	P2	B1	0.5	50

Table 3.1 (continued) Bath ingredients and parameter for experimental studies.

CC5-26	5% HF	H_3PO_4	S2	P2	B1	0.25	50
CC5-27	5% HF	H_3PO_4	S2	P2	B2	1	50
CC5-28	5% HF	H_3PO_4	S2	P2	B2	1	60
CC5-29	5% HF	H_3PO_4	S2	P2	B1	1	45

*In electroless plating bath setup in (G) refers to glass beaker, (PP) refers to polypropylene beaker.

Table 3.2 Electroless silver plating baths.

Name of Chemical		**Concentration**		
		B1	**B2**	**B3**
Silver Source	$AgNO_3$	1.67 g/L	1.67 g/L	1.67 g/L
Reducing Agent	$N_2H_4.H_2O$	0.35 g/L	0.35 g/L	0.35 g/L
Complexing Agent	NH_4OH	200 mL/L	200 mL/L	200 mL/L
Chelating Agent (0.15 M)	$C_{10}H_{18}N_2Na_2O_{10}$	--	100 mL/L	200 mL/L
Stabilizer	$(NH_4)_2CO_3$	70 g/L	70 g/L	70 g/L
Operating Parameters				
Temperature (°C)		45, 50*, 55, 60, 70, 80	50, 60, 70, 80	50, 60, 70, 80
pH		9.5-11.0	9.5-11.0	9.5-11.0
Duration		0.25*, 0.50*, 1*, 1	1	1

3.2.1 Etching

After the initial roughness values were recorded, grinding and acid etching were performed to see the effect of different roughening mechanisms on surface roughness. After roughening processes, final roughness values were recorded. XRF-EDS analysis

were done to obtain compositional changes in ceramic after HF etching and SEM imaging used for morphological analysis for ceramics. Table 3.3 include the etching method and type of material that used.

Table 3.3 Types of etchants.

Etchant type	Grid	Concentration (wt. %)
SiC Sandpaper	180,240,320	-
HF (70% purity)	-	5
HF (70% purity)	-	10

3.2.2 Cleaning and Degreasing

Cleaning and decreasing processes were carried out in two-step as alkaline and acidic solutions. Firstly, ceramics were cleaned and neutralized in alkaline solution (1.25 M NaOH) in ultrasonic bath at 60°C for 5 minutes [121] and then immersed in acidic solution after rinsing in distilled water. Acid cleaning was carried out in an ultrasonic bath for 5 minutes at 60°C according to the recipe shown in Table 3.4. In order to obtain an appropriate process, initial and final composition analyses and roughness measurements of ceramics were performed.

Table 3.4 Acidic degreasing, etching compositions.

Type of Acid	Concentration
H_2SO_4 (95-97%)	2 M
HCl (37%)	2 M
H_3PO_4 (85%)	2 M

3.2.3 Sensitization

The first step of metallization procedure for nonconductive surface, which is detailed in Section 2.5, is sensitization. As shared in Table 3.5, two different bath compositions were used for sensitization process. Free Sn^{+2} ions in sensitization bath adhere to the locations created by etching. Sensitization processes were completed in 5 minutes at 30°C for S1 and S2.

Table 3.5 Sensitization baths and working temperatures.

Bath Name	Composition		Temperature (°C)
S1	**$SnCl_2$**	**HCl (37%)**	30
	5 g/L	81.9 mL/L	
S2	**$SnCl_2$**	**HCl (37%)**	30
	11.3 g/L	15 mL/L	

3.2.4 Activation

The second stage of the metallization procedure is Pd activation. At this stage, free Sn^{+2} ions oxidize and reduce the Pd ions as in Equation (2.7). There are two different concentrations for activation baths as shared in Table 3.6. After the activation, substrate was rinsed with distilled water and immersed in the electroless silver plating bath. In plating bath, as a result of the reaction between metal ion source and reducing agent, free Ag ions are reduced and attached to the ceramic surface thanks to active sites (Pd-sites). Activation process was completed in 3 minutes at 40°C for P1 and at 30°C for P2.

Table 3.6 Activation baths and working temperatures.

Bath Name	Composition		Temperature (°C)
P1	**$PdCl_2$**	**HCl (37%)**	40
	0.5 g/L	81.9 mL/L	
P2	**$PdCl_2$**	**HCl (37%)**	30
	2.5 g/L	25 mL/L	

3.2.5 Elemental Characterization and Average Coating Thickness, Surface Morphology, Phase Formation and Conductivity Analysis

For the measurement of the average coating thickness, XRF-thickness mode analysis was used. Cross-section thickness analyses were performed by Optical Microscope (Nikon LV150N) and Digital Microscope (Nikon ShuttlePix P-400Rv) to verify the XRF results.

Phase analyses of coated ceramics were obtained using X-ray diffraction (XRD) with CuKα radiation. XRD data was taken between 2θ = 10-110° with step size of 0.02° and scanning speed of 2°C/minute. SEM (FEI Nova NanoSEM 430) analyses were performed to examine the surface quality of the silver coating deposited on the ceramic surface. In addition, compositional analyses were performed by SEM-EDS on electroless coated silver surface.

Sheet resistivity measurements were performed with 4-point probe resistivity system (Lucas/Signatone Four Point Probe-302).

CHAPTER 4

RESULTS AND DISCUSSION

After optimum pretreatment processes were (etching, alkaline-acid cleaning and metallization) selected, electroless silver plating was carried out on the B1, B2 and B3 bath compositions. The maximum plating rates were obtained for B1 as 9.07 µm/hr at 50°C; for B2 as 5.09 µm/hr at 50°C and for B3 as 13.49 µm/hr at 60°C.

4.1 Characterization of Ceramics

XRD result of ceramics sintered at 1400°C for 4 h is given in Figure 4.1. As can be seen, $CaTiO_3$-type orthorhombic perovskite structure was observed [30]. Relative density of ceramics was calculated as >97% and ceramics had <1% water absorption and apparent porosity and results are given in Table 4.1. These results shows that ceramic fabrication processes were successfully completed. EDS elemental analysis is shown in Figure 4.2a. Figure 4.2b and Figure 4.2c shows morphological analysis of bulk ceramic surface. After the morphological analyses, it was determined that the grain size was between 1 and 6 µm. The spaces between the grains also caused a 3% decrease in density.

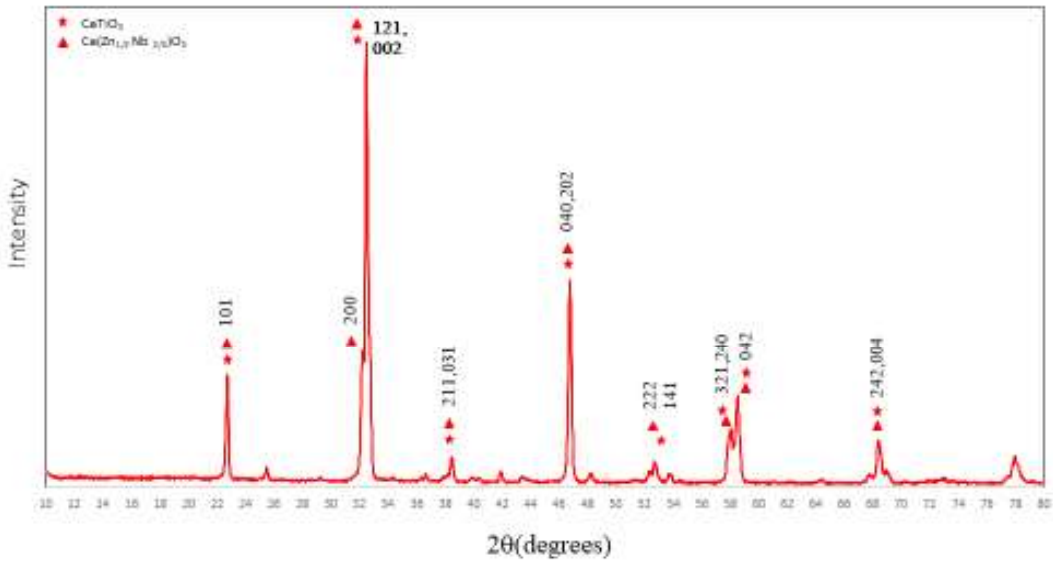

Figure 4.1 XRD spectrum for CT-CZN x32.

Table 4.1 Bulk density, relative density, water absorption and apparent porosities of CT-CZN x32 ceramics.

No	W_d (g)	W_s (g)	W_w (g)	BD$^{\#}$ (g/cm^3)	RD* (%)	WA$^{\#}$ (%)	AP$^{\#}$ (%)
1	0.28	0.21	0.28	4.156	97.03	0.06	0.28
2	0.30	0.23	0.30	4.167	97.27	0.03	0.13
3	0.30	0.23	0.30	4.159	97.08	0.13	0.54
4	0.27	0.21	0.27	4.193	97.89	0.07	0.29
5	0.28	0.21	0.28	4.140	96.64	0.21	0.87
6	0.27	0.21	0.27	4.176	97.48	0.10	0.44
7	0.30	0.23	0.30	4.186	97.72	0.06	0.27
Average					**97.30**	**0.09**	**0.40**

Values that indicated with '$^{\#}$' were calculated as follows with dry weight W_d, wet weight W_w and suspended weight W_s:

$$Bulk\ Density\ (BD)\ (\frac{g}{cm^3}) = \frac{W_d}{W_w - W_s} * 0.99 \quad \textbf{(4.1)}$$

$$Water\ Absorption\ (\mathrm{WA})(\%) = \frac{W_w - W_d}{W_d} * 100 \quad \textbf{(4.2)}$$

$$Apparent\ Porosity\ (AP)\ (\%) = \frac{W_w - W_d}{W_w - W_s} * 100 \quad \textbf{(4.3)}$$

Values of RD (Relative Density) that marked with '*' were calculated with respect to 4.284 g/cm^3 [30].

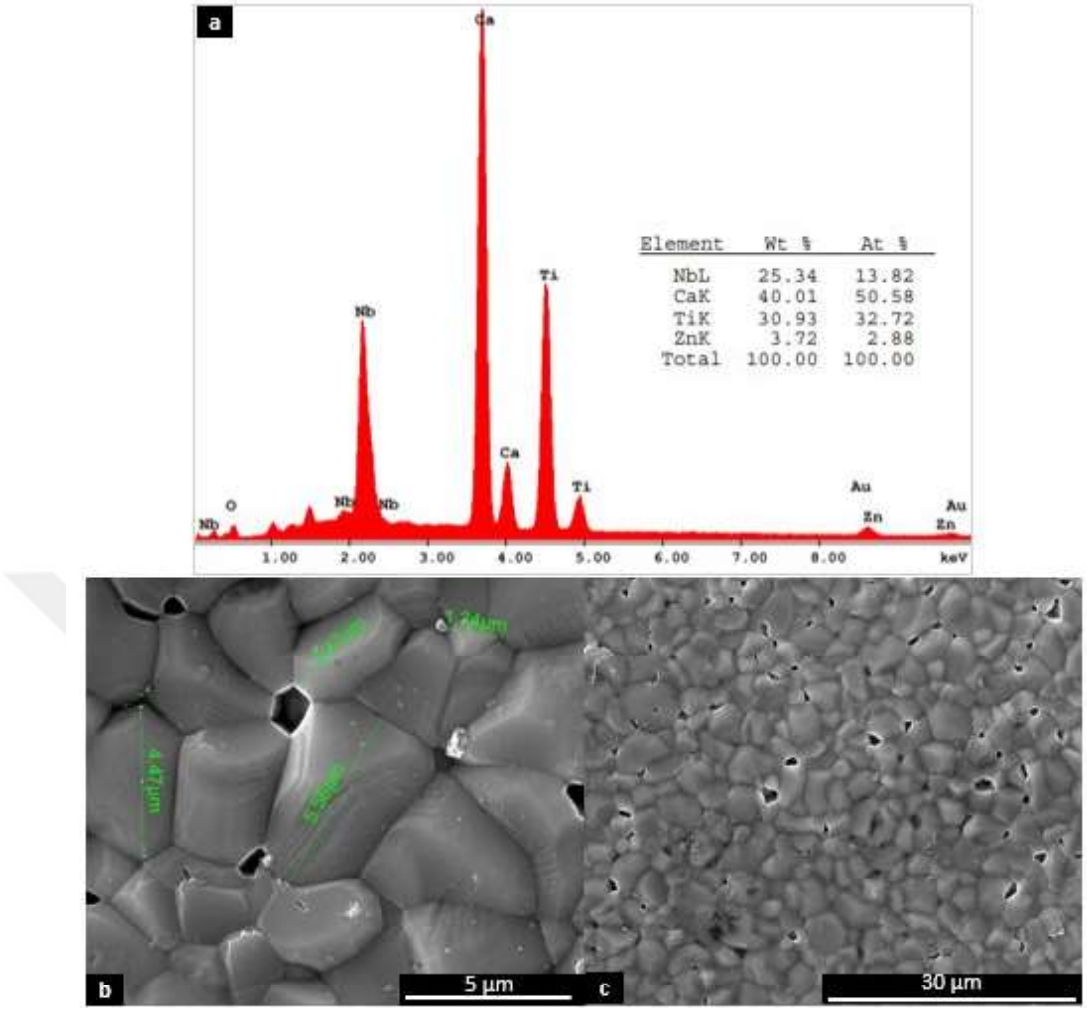

Figure 4.2 Surface analysis for bulk CT-CZNx32 ceramics with a) EDS elemental analysis b) SEM imaging in 20000x, c) SEM imaging in 5000x magnification.

4.2 Effect of Etching Type on Ceramic Composition and Plating Rate

In order to increase adhesion of silver ions on ceramic surfaces, it is necessary to increase the surface area. The steps of increasing the surface area can be considered under the heading of etching. In the experiments carried out in this context, the ceramic composition was analyzed by XRF-EDS after HF etching. The same process applied before and after alkaline-acid cleaning steps. Table 4.2 and Table 4.4 show the results in compositions. In addition, roughness values recorded before and after etching and cleaning steps. Proper steps selected according to the XRF results.

4.2.1 Alkaline and Acid Cleaning

After alkaline-acid cleaning steps final compositions were examined. After cleaning with 2 M sulfuric acid cleaning 0.5% decrease observed in Zn concentration. This is a result of $ZnSO_4$ formation into the solution. As a result of 2 M HCl cleaning step, 0.71% decrease observed in Ca because of the formation of $CaCl_2$ salt. However, in the analysis performed after 2 M H_3PO_4 acid cleaning, it was determined that the ceramic composition did not damage from acid. Therefore, the appropriate alkaline cleaning bath was determined as 1.25 M NaOH and acid cleaning bath as 2 M H_3PO_4. While the roughness increase with cleaning of 2 M HCl, considering the 0.71% Ca decreasing, this method was not selected (Table 4.2). Figure 4.3 shows the initial and final roughness values of ceramics before and after acid cleaning steps.

Table 4.2 Change in composition of ceramic substrate after acid cleaning.

Type of Acid (2 M)	Elements	Initial Composition	Decrease in Composition	Change in Roughness (%)
H_2SO_4	Ca	42	0	+14
	Ti	31	0	
	Nb	22	0	
	Zn	3.5	**- 0.50**	
	Zr	0.5	0	
HCl	Ca	43.24	**- 0.71**	+66
	Ti	32.2	0	
	Nb	21.29	0	
	Zn	2.91	0	
	Zr	0.36	0	
H_3PO_4	Ca	42.97	0	-59
	Ti	31.93	0	
	Nb	21.58	0	
	Zn	3.16	0	
	Zr	0.37	0	

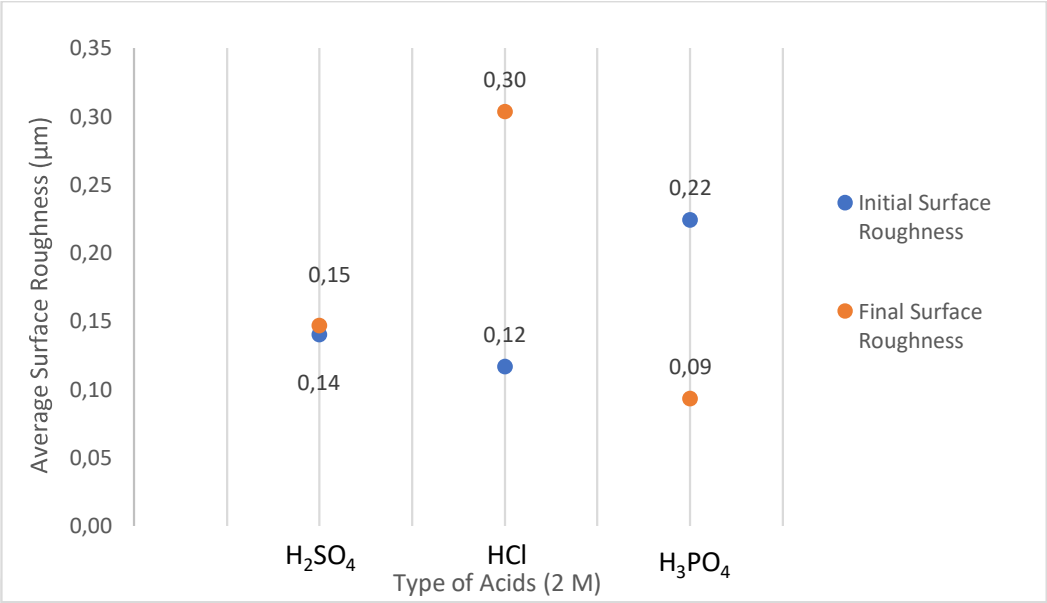

Figure 4.3 Effects of type of acids on surface roughness.

4.2.2 Etching Procedure with HF and Sandpaper Grinding

Etching process was applied to increase surface area and to create micro-pores inside the ceramic with diffusion. Experiment 4 (Sample ID: CC5-5) was done to see the effect of roughening. As a result, lack of roughness lead to poor adhesion and depletion of silver agglomerate (Figure 4.4). In this context, HF etching and sanding processes were performed to increase the surface roughness. According to the measurements which was done by profilometer, maximum roughness value was obtained from 240 grid SiC sandpaper grinding and then 5% HF etching.

Figure 4.4 Digital microscope imaging of CC5-5.

Table 4.3 shows the relation between roughness, metallization process and on coating thickness.

Table 4.3 Etchant type and change in roughness.

Etchant type	Sample ID	Grid	Concentration (wt. %)	Increase in Roughness (%)
None	CC5-5	-	-	-
HF	CC5-6	-	5	39
HF	CC5-7	-	10	0
SiC Sandpaper	CC5-8	180	-	0
SiC Sandpaper	CC5-10	240	-	77
SiC Sandpaper	CC5-11	320	-	7

As a result of the analysis performed after 5% HF etching (see Table 4.4), it was determined that there was no change in the ceramic composition. However, when the

HF concentration increased to 10%, a decrease of Ti concentration as approximately 2% was observed. This reduction occurs with the formation of $[TiF_6]^{3-}$ [122] ion when titanium is exposed to a dilute HF acid.

Table 4.4 Compositional analysis for ceramic concentration after HF etching.

Concentration of HF (wt. %)	**Initial Composition (%)**		**Change in Composition (%)**
5	Ca	42.94	0
	Ti	31.8	0
	Nb	21.5	0
	Zn	3.3	0
	Zr	0.39	0
10	Ca	43.33	0
	Ti	32.11	**- 1.71**
	Nb	21.47	0
	Zn	2.71	0
	Zr	0.38	0

Figure 4.5 gives SEM image after 5% HF etching of Experiment 22. Grain size of less than 5 μm can be formed by this process and the produced micro-pores increase the adhesion by providing an advantage in the metallization stage. Although, it was observed that SiC grinding increased the surface roughness, adhesion was low in the microstructural analysis of coating. As seen in Figure 4.5, it was observed that the roughness of the initial surface decreased after HF etching and enabled the formation of active regions on the flat surface during the metallization. Figure 4.6 includes the cross-section OM and SEM images of Experiment 14. According to these images, 5% HF can diffuse into depths of 27.13 to 35.02 μm.

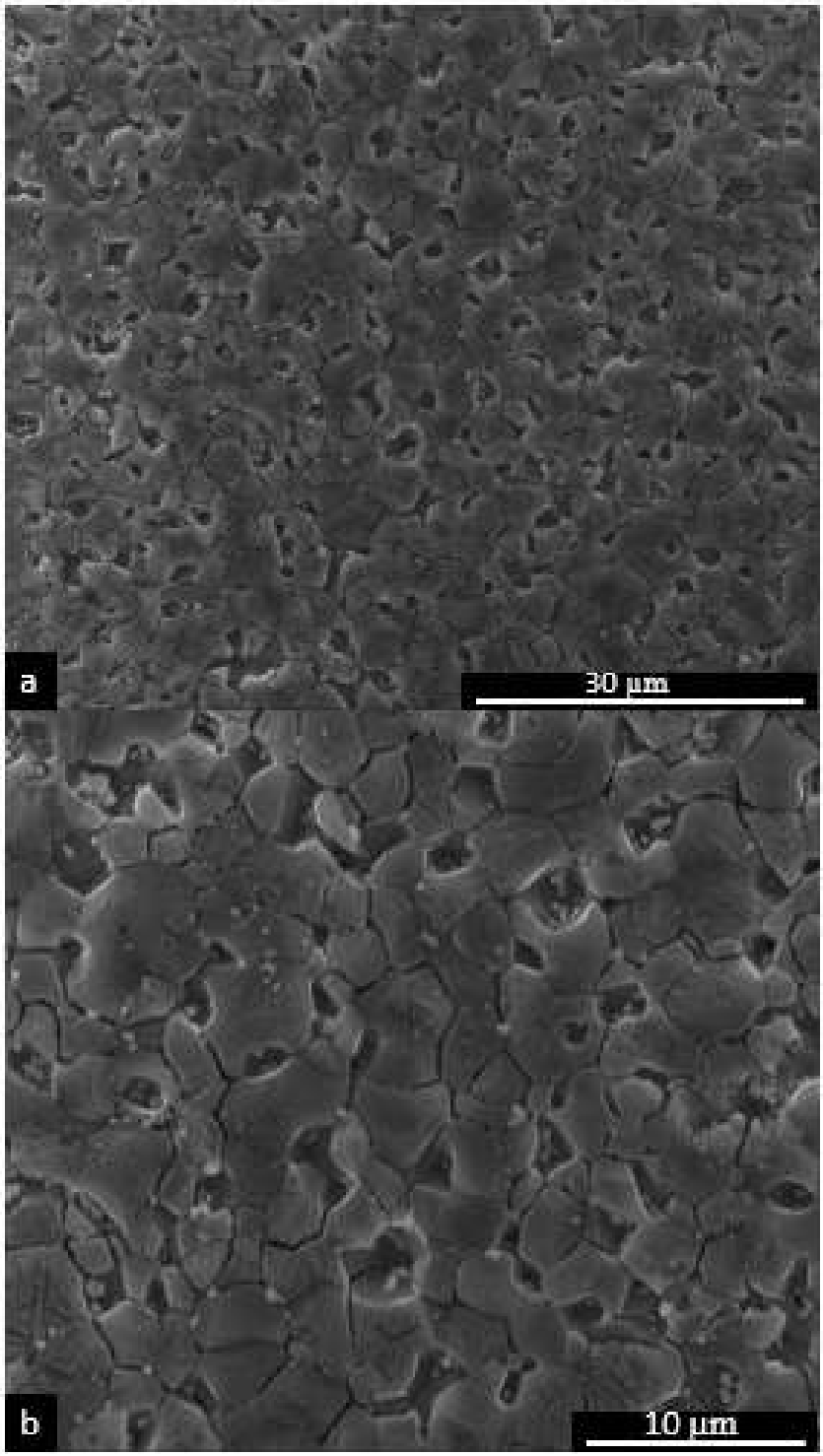

Figure 4.5 Surface morphology analyze for 5% HF ceramic surface with SEM a) 2000x magnification b) 4000x magnification.

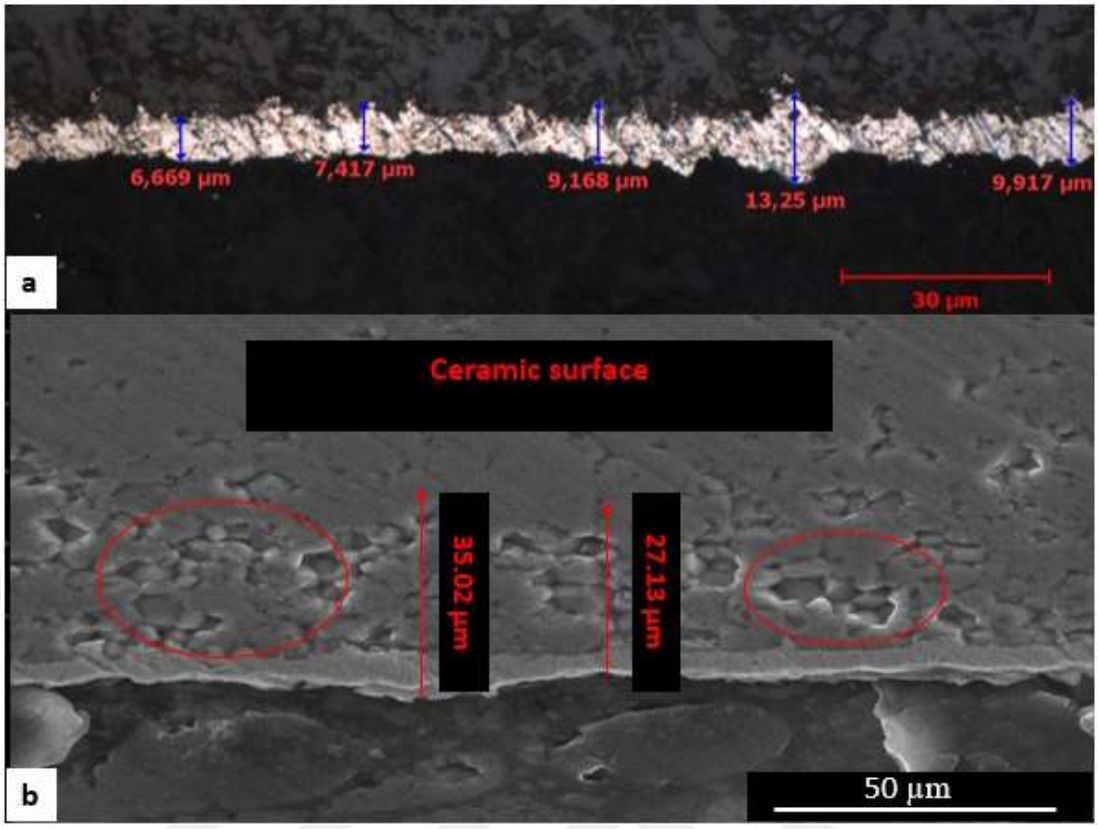

Figure 4.6 Cross section images in a) 1000x magnification with OM, b) 1200x magnification with SEM.

4.3 Effect of Metallization Procedure on Plating Rate

The details of the metallization procedure completed in 2-stages were explained in Section 2.5 and metallization baths were given in Section 3.2.3 and 3.2.4. Time of sensitization process was determined as 5 minutes for each experiment. For activation process, time was selected as 3 minutes to obtain maximum number of Pd nuclei as mentioned in Section 2.5. SEM-EDS analysis, given in Figure 4.7 was completed on the ceramic surface after metallization process (S2+P2) to examine active sides for Pd. After the morphological analysis, nano-sized tin and palladium particles were detected. The active Pd surfaces observed on the flat surfaces obtained after 5% HF etching may decrease by shedding from the surface within the period until analysis. In this context, it was decided to enter the electroless silver plating bath immediately after the metallization process. For the coating thickness analysis, the bath temperature kept

constant at 55°C and the ceramic was hold in plating bath for 1 hour. Table 4.5 shows the effect of metallization procedure on coating thickness.

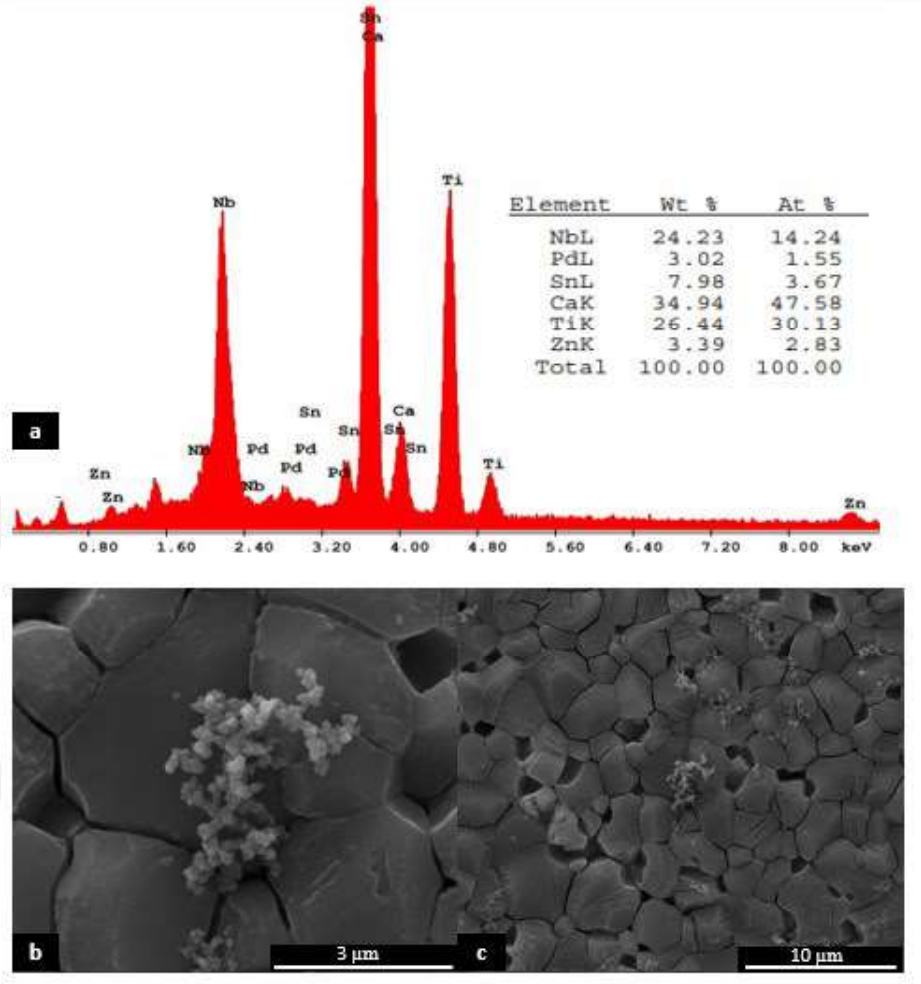

Figure 4.7 a) EDS analysis and SEM images in b) 40000x and c) 10000x magnification of metallized ceramic surface.

Table 4.5 The effect of metallization procedure on coating thickness obtained at 55°C.

ID	Etching Type	Sensitization	Activation	Coating Thickness (µm)
CC5-6	5% HF	S1	P1	Unsuccessful
CC5-9	240 Grid SiC	S1	P1	1.47
CC5-10	240 Grid SiC	S2	P2	2.37
CC5-12	5% HF	S2	P2	4.61
CC5-13	5% HF	-	P2	Unsuccessful

Coating thickness was measured from CC5-9 as 1.47 μm. Etching and metallization were completed with 240 sandpaper grinding and S1+P1 baths, respectively. However, for CC5-10 the coating thickness obtained was 1.6 times thicker with S2+P2 metallization procedure (Figure 4.8b). After five percent HF etching, average coating thickness measured as 4.61 μm with S2+P2 (Figure 4.8d), however S1+P1 metallization performed under same conditions was not successful because silver could not adhere to the surface (Figure 4.8c). Only palladium activation applied on CC5-13 (Figure 4.8e) resulted in lack of adhesion for silver plating because palladium ions could not adhere to the surface without reaction between tin and palladium ions. Average diameter of spherical tin is 28 nm and it is larger than palladium [123]. Therefore, tin atoms that are tightly placed in the <5 μm micro-pores formed after HF perform an oxidation reaction with palladium, revealing a conductive surface (Figure 4.7). In this context, the two-step metallization process was selected as S2 (11.3 g/L $SnCl_2$ and 15 mL/L HCl and P2 (2.5 g/L $PdCl_2$ and 25 mL/L HCl) to obtain high coating thickness. The increase in amount of $SnCl_2$ in S2 and $PdCl_2$ in P2, as well as the decrease in the concentration of HCl in S2 lead to higher coating thicknesses instead of 12 M HCl [124] for sensitization bath, 0.5 M HCl solution was prepared to reduce the acid concentration and bring the pH to more efficient working conditions [43].

As seen in Figure 4.8b and Figure 4.8d, HF etching process is preferred in terms of applicability and obtaining a base for active surface formation.

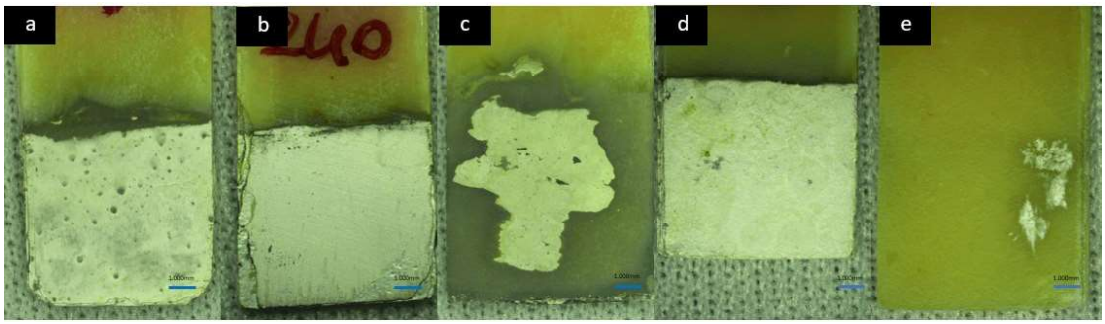

Figure 4.8 Digital microscope imaging for experiment no a) CC5-9, b) CC5-10, c) CC5-6, d) CC5-12, e) CC5-13.

4.4 The Effects of Temperature, Time and Chelating Agent on Plating Rate

According to silver plating bath dynamics, reaction rate increases as the temperature increases, so coating thickness changes with respect to temperature change. Increasing temperature results in aggressive behavior of bath and causes silver loss due to the agglomeration and contamination on the beaker walls. In order to observe the relationship between the coating thickness and temperature, experiments were performed with B1, B2 and B3 at different temperatures and time. Table 4.6 includes the experiments and coating thickness analyzes. Pretreatment process was the same for all experiments; alkaline cleaning with 1.25 M NaOH, acid cleaning with 2 M H_3PO_4, etching with 5% HF and metallization with S2+P2 baths.

Table 4.6 Relation between temperature-coating thickness and time-coating thickness.

ID	Bath	Temperature (°C)	Time (min)	Coating Thickness (µm)
CC5-29	B1	45	60	2.05
CC5-26	B1	50	15	1.99
CC5-25	B1	50	30	5.43
CC5-15	B1	50	60	9.07
CC5-27	B2	50	60	5.09
CC5-12	B1	55	60	4.61
CC5-24	B3	50	60	2.90
CC5-14	B1	60	60	2.04
CC5-28	B2	60	60	4.29
CC5-23	B3	60	60	13.49
CC5-22	B1	70	60	0.88
CC5-18	B2	70	60	4.12
CC5-19	B3	70	60	8.44
CC5-21	B1	80	60	0.85
CC5-20	B2	80	60	3.48
CC5-17	B3	80	60	6.37

Figure 4.9 shows the relationship between plating rate (µm/hr) and temperature for B1. Maximum plating rate was obtained as 9.07 µm/hr at 50°C. It is reported in the literature that, a coating thickness of 2 µm was achieved at 83°C in 1 h [88]. The reaction rate increases with increasing bath temperature and become too aggressive as mentioned earlier. When the bath temperature reached the specified temperature as published in literature [88], Ag atoms started forming a dust and clinched on existing silver particles instead of depositing onto the active ceramic surface. However, with the same bath composition, the coating thickness was 10 times thicker at 50°C.

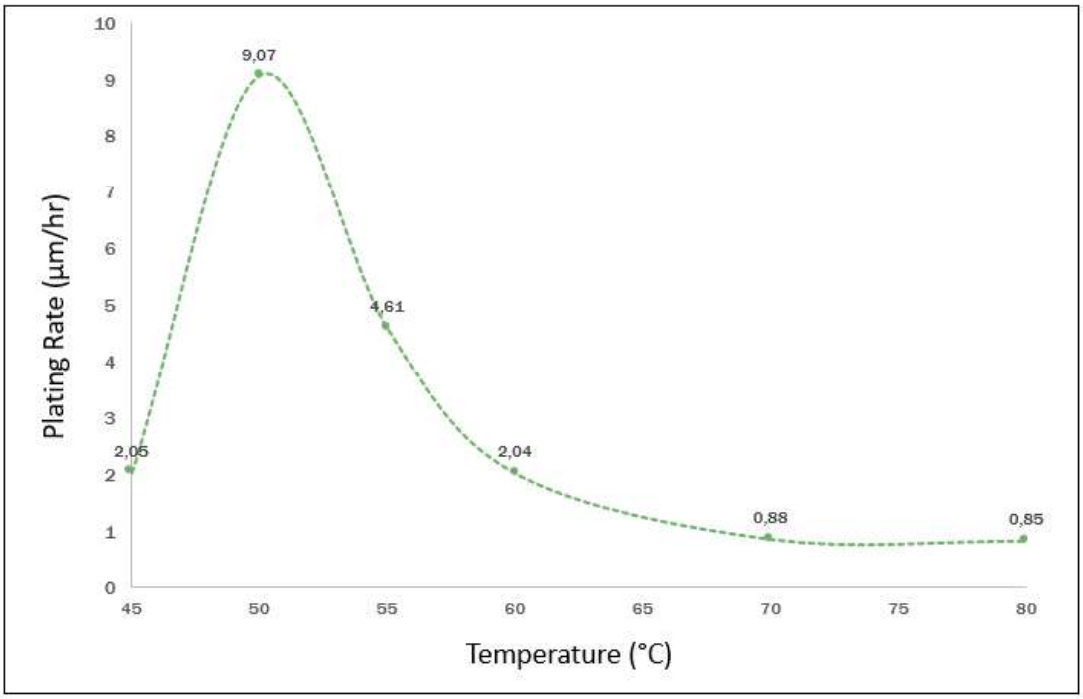

Figure 4.9 Relation between temperature and plating rate for B1.

The relationship between the coating thickness and the time was observed with the 15 minutes, 30 minutes and 60 minutes experiments carried out at 50°C. Figure 4.10 includes the coating thickness versus time relationship.

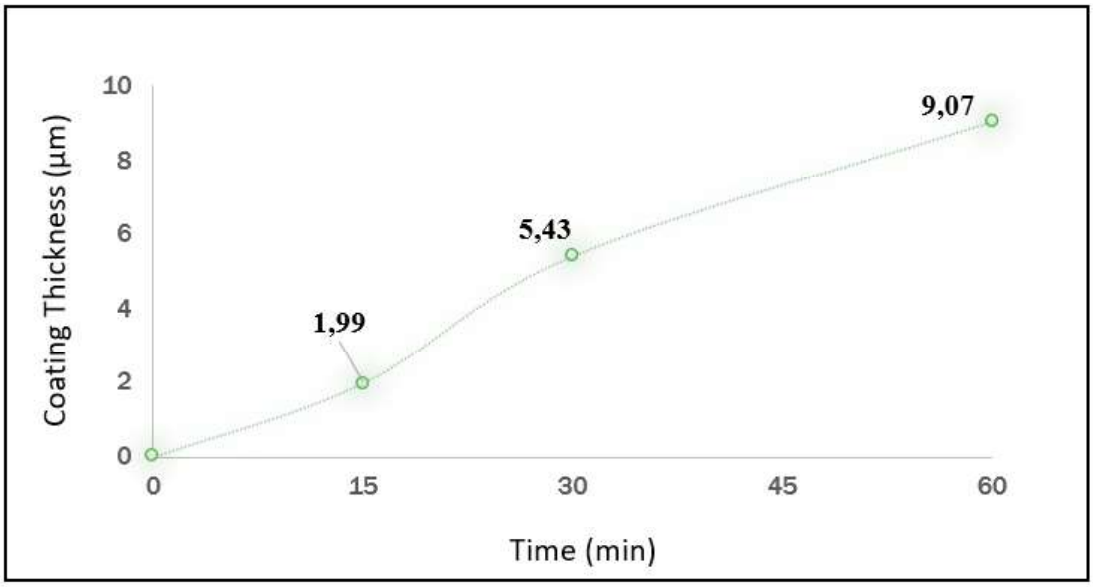

Figure 4.10 Time and coating thickness relation at 50°C.

Coating thickness was measured as 1.99 µm after 15 minutes at 50°C. However, when the time was doubled, it was observed that the deposition accelerated and the coating thickness reached 5.43 µm rather than a linear increase. An intermediate product is formed with the reaction between silver nitrate and ammonium hydroxide in electroless silver plating bath. Silver metal is obtained as a result of the reaction by product of the reducing agent and intermediate product. Therefore, lower reaction rate between intermediate product and the reducing agent could have caused the lower plating rate at the fifteenth minute. In this context, after 30 minutes the coating thickness increased by 2.72 times and was recorded as 5.43 µm. However, at the end of the first hour, the rate of increase in coating thickness slowed down and 9.07 µm thickness obtained (Figure 4.11). Since no ion concentration enhancer was added during the coating period, the bath was exhausted and its efficiency decreased.

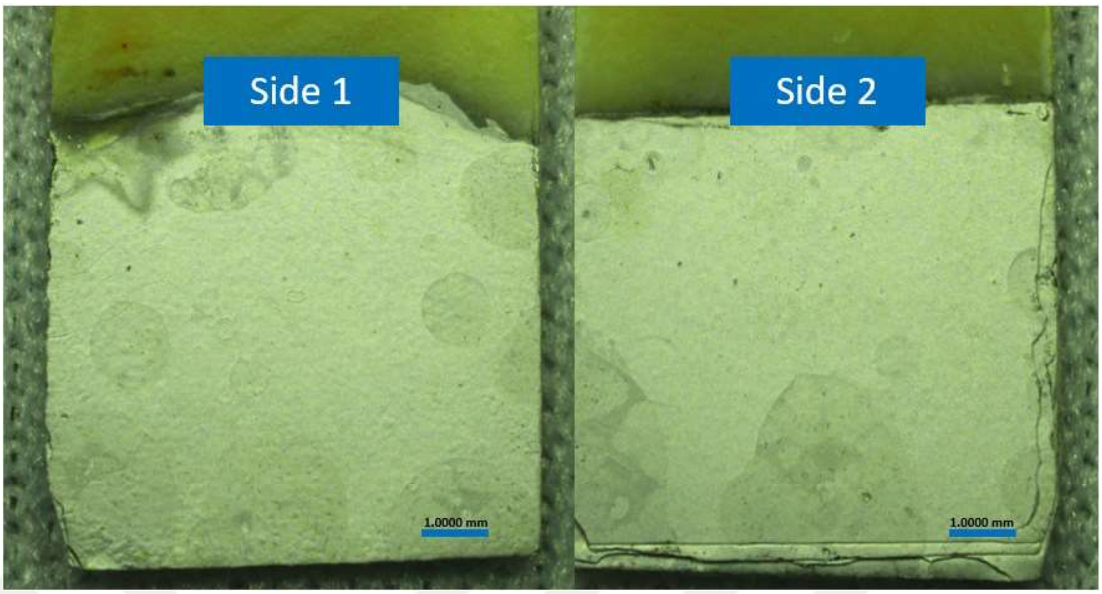

Figure 4.11 Digital microscope imaging for CC5-15.

4.4.1 Effect of Chelating Agent on Plating Rate

Chelating agents were added to the bath to prevent potential toxic complexes that may occur in the bath at high and low temperatures. In addition, EDTA is added to the electroless silver plating bath to prevent deposition to the beaker. At low temperatures, EDTA adversely affects the reaction rate but at high temperatures, as it contributes to the stabilization of the bath, it delays the formation of agglomeration and increases the adhesion to the catalytic active ceramic surfaces. The graphs in Figure 4.12 and Figure 4.13 are the tangible proof for this situation.

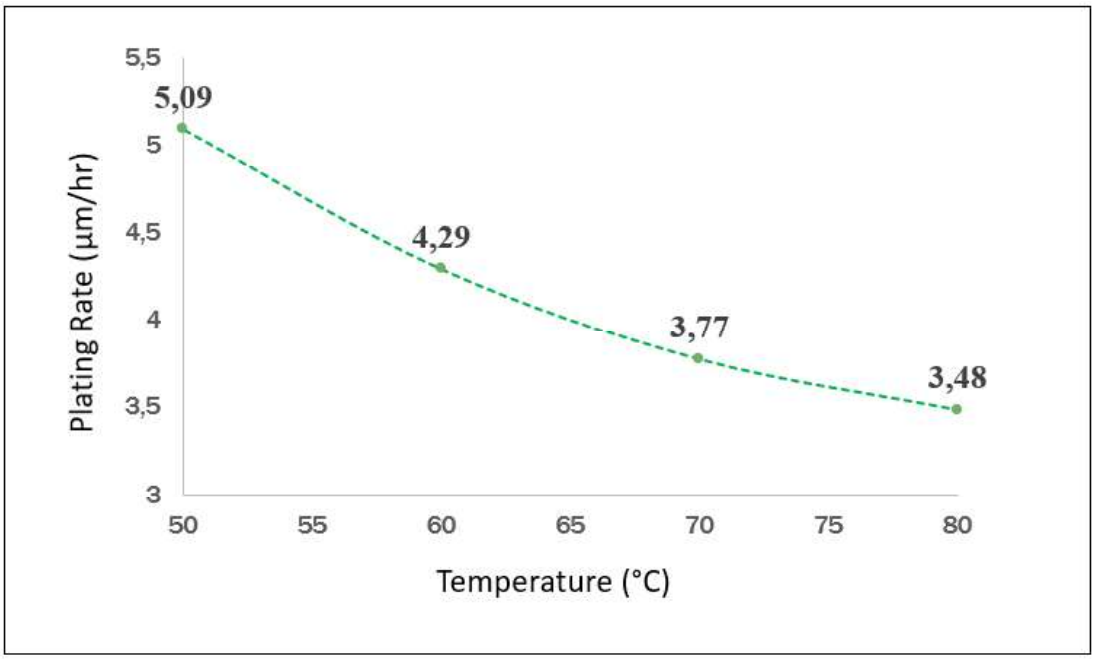

Figure 4.12 Plating rate and temperature relation of bath 2.

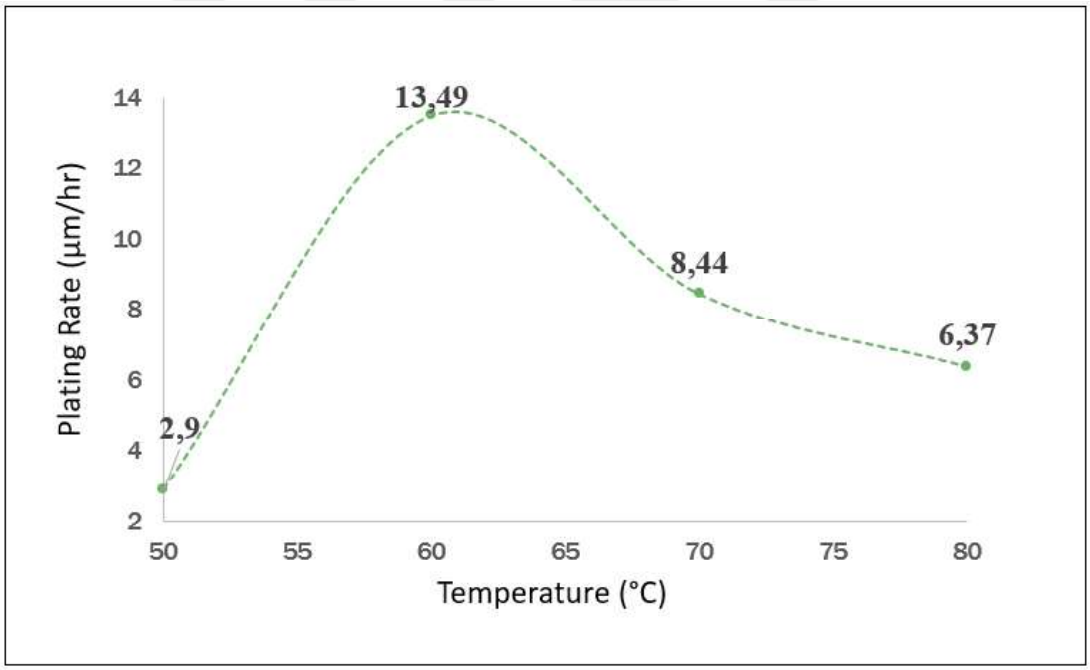

Figure 4.13 Plating rate and temperature relation of bath 3.

The effect of the amount of EDTA on the coating thickness was investigated by experiments carried out at constant temperature. Figure 4.14 shows the effect of chelating agent on plating rate at constant temperature. According to the graphs,

decrease in coating thickness was caused by increasing amount of EDTA in plating bath at 50°C. The reason for this decrease is the slowdown of the silver deposition rate due to the added chelating agent making the bath more stable, but it should not be ignored that the increase in coating thickness increases with time. Contrary to the decrease in coating thickness at 50°C, with the increase in temperature and the added chelating agent, the bath tended to make a thicker coating at 60°C. The maximum coating thickness was recorded as 13.49 µm with the added 20 mL of 0.15 M EDTA. While the increase in coating thickness in B3 was 2.23 times higher than B2 at 70°C, it was 1.83 times higher at 80°C. It was observed that the reaction became easier with the increase in temperature, but the added amounts were probably insufficient at 70°C and 80°C.

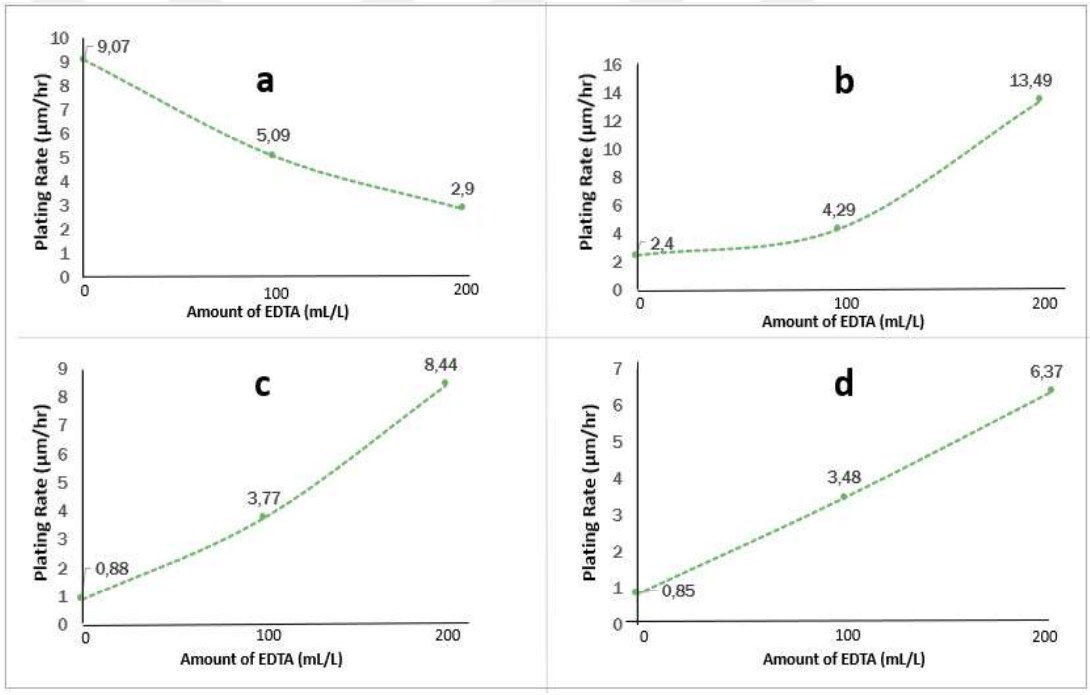

Figure 4.14 Relation between plating rate and B1, B2 and B3 at a)50°C, b)60°C, c) 70°C, d) 80°C.

4.5 Coating Properties

Phase formation analysis of the coating was done by XRD with Sample ID CC5-23. Coating thickness was measured as 13.49 µm after plating at 60°C for 1 h with B3. Matching was made according to the PDF card number (JCPDS file no: 04-0783) and it was observed that the phases overlap. Figure 4.15 include phase formation analysis

for silver coating and 100% intensity was observed at 2Θ ≈ 38.12 ° when matched with JCPDS card. Since the (111) plane has the lowest surface energy, it is concluded that when the amount of chelating agent was optimum, the preferred growth was on (111). Also, the dominance of (111) plane resulted in pyramidal growths as shared in Figure 4.16.

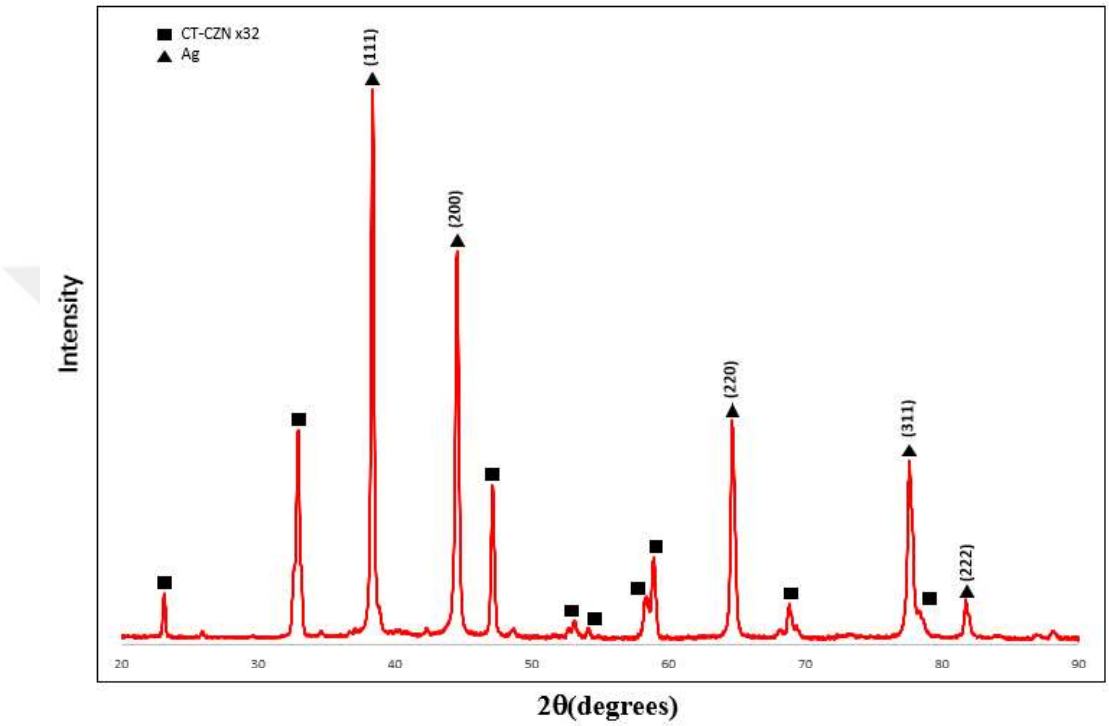

Figure 4.15 Phase formation analysis for CC5-23.

As a result of the EDS analysis performed on the coating, 100% silver was detected and shared in Figure 4.17. Figure 4.18 includes the EDS analysis of the ceramic-metallic coating interface. The purpose of the analysis was to detect residual palladium on the ceramic surfaces immersed in the bath after the metallization procedure, but as a result of the analysis, no Pd atoms were found except for Ca, Ti, Nb, Zn and Ag from electroless metal coating.

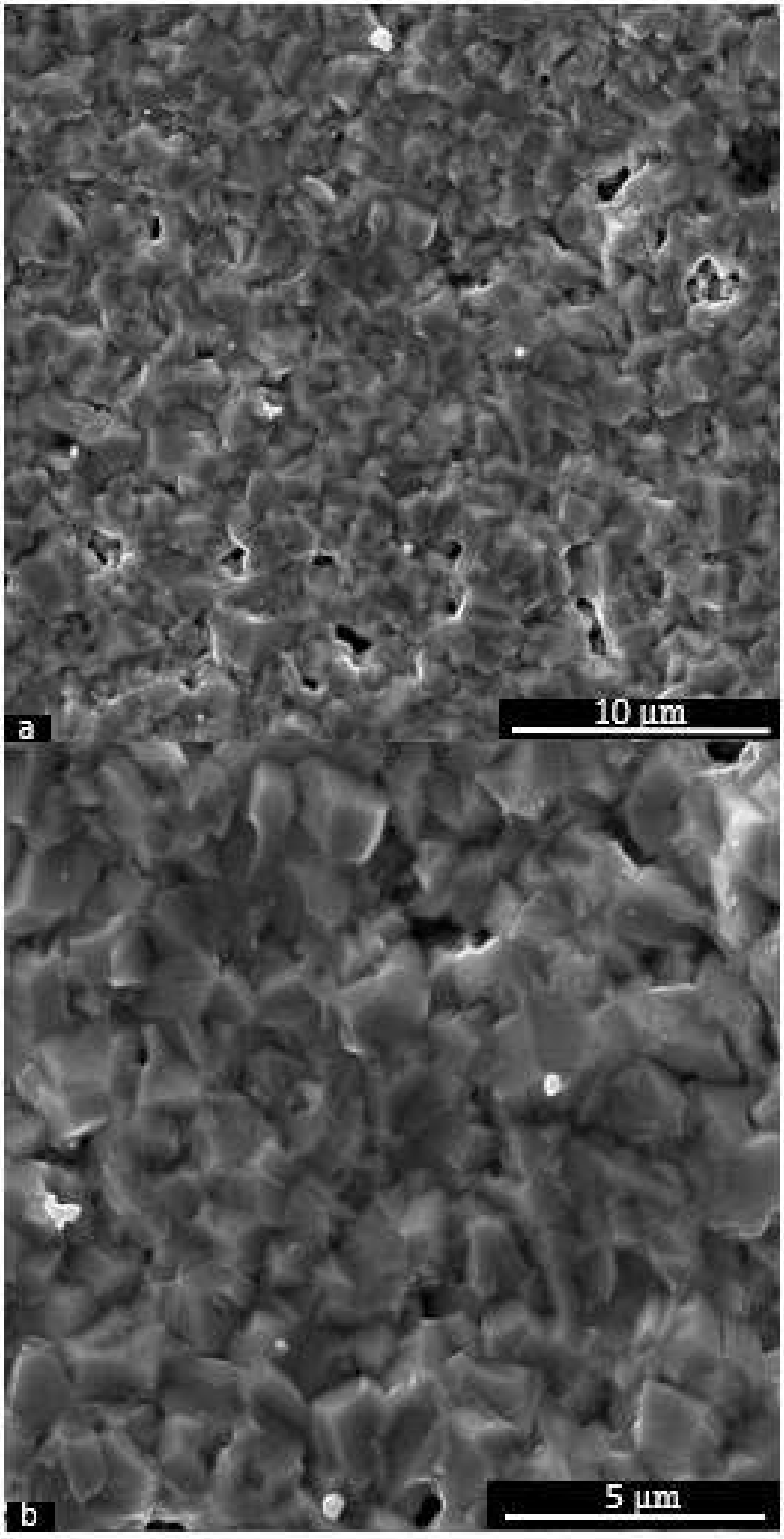

Figure 4.16 SEM images of electroless silver plating in a) 10000x, b) 20000x magnification.

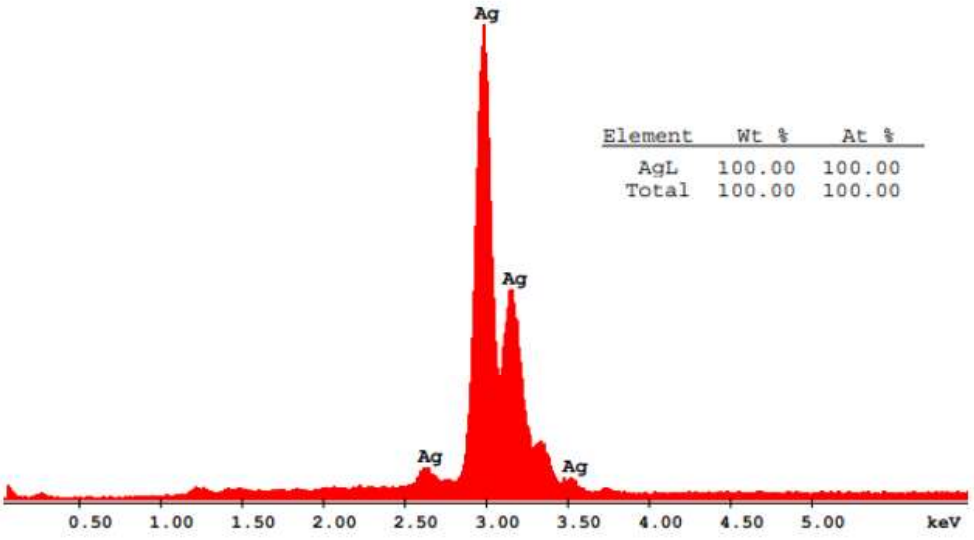

Figure 4.17 EDS analysis of electroless silver plating.

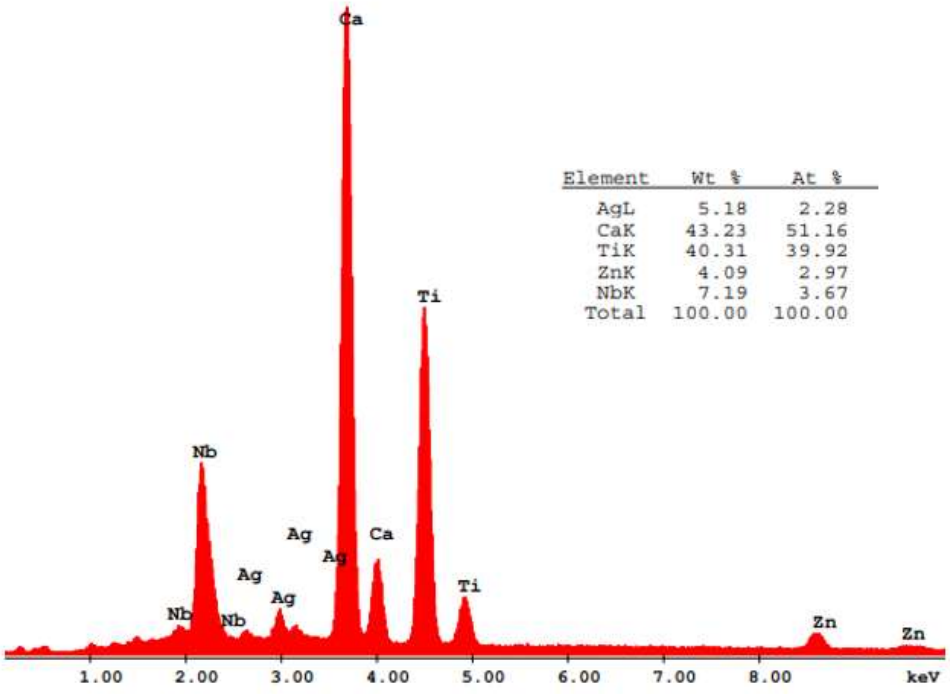

Figure 4.18 EDS analysis in cross-section between silver and ceramic surface.

According to sheet resistance measurements from 4.12 µm thickness (ID: CC5-18) silver coating, conductivity of silver was calculated as 1.8×10^7 S/m.

CHAPTER 5

CONCLUSION

0.68CT-0.32CZN ceramic composition that obtained with calcination and it was weighing 45% by weight of the tape casting solution and pouring with rate of 250 μm at 5 cm/sec and 80 μm thickness with homogeneous and pseudoplastic behavior. Relative density measurements from bulk ceramics was obtained as higher than 97%. Also, less than 1% water absorption and open porosity were obtained from bulk ceramics. As a result of the phase formation analysis, orthorhombic perovskite structure was observed. After the profilometer measurements of the ceramic surface with a 5 μm type, the average roughness value was recorded as 0.13 μm.

Surface morphology analysis shows micro-pores that formed by 5% HF etching and this situation increased the retention of palladium in the metallization step. Morphological analysis made after metallization step; it was observed that the image formed on the substrate was in the same direction as the silver metal attached to it. The results obtained after the experiments;

- According to the data obtained from the XRF-EDS results and the coating thickness measurement, the appropriate etching process selected as 5% HF.
- According to the repeated XRF-EDS results, it was decided to complete the alkaline-acid cleaning with 1.25 M NaOH and then with 2 M H_3PO_4, respectively.
- 2-step metallization process chosen because of result in insufficient adhesion of only palladium activation.
- According to thickness measurement and visual adhesion inspection performed within the scope of the metallization procedure, the proper sensitization bath selected as S2; the proper activation bath selected as P2.

Parameters have been developed within the scope of increasing the coating thickness and optimizing the bath in the silver nitrate-based electroless bath composition used as a silver ion source. From the experimental studies, the following conclusions were drawn:

- Electroless silver plating carried out with B1 for 0.25 hours, 0.5 hours and 1 hour at 50°C and recorded as 1.99 μm, 5.43 μm and 9.07 μm, respectively. The maximum coating thickness was 9.07 μm after 1 hour. However, the coating thickness increase rate is not proportional with the increase of the time, because the ion concentration in the interior decreases with the deposition of silver. The achieved coating thickness of 2 μm at 83°C for 1 hour stated in the literature [88] was reached after 15 minutes at 50°C. Since the bath stabilization was disrupted at 83°C, silver agglomeration occurred and silver did not attach to the ceramic surface.

- The maximum coating thickness of 5.09 μm obtained after 1 hour at 50°C with B2. However, it has been observed that the amount of chelating agent added in slows down the reaction somewhat. Increasing the time over 1 hour at the same temperature (50°C) and bath composition will result in a positive increase in coating thickness.

- 12 μm metal layer is requested in dielectric resonator ceramic systems. With the increasing EDTA amount and temperature, the targeted at least 12 μm coating thickness was achieved after 1 hour at 60°C as 13.49 μm with B3.

- The maximum coating thickness with B3 obtained after 1 hour at 60°C. This value is followed by 8.44 μm at 70°C and 6.37 μm at 80°C, respectively. Since the increase in the amount of chelating agent added slowed down the reaction rate at 50°C, it had a negative effect on the coating thickness.

- At higher temperatures (i.e., at 70°C and 80°C), an increase in coating thickness can be observed with increasing the amount of chelating agent included in the bath composition.
- After the phase formation analysis, a one-to-one match observed with the JCPDC file no 04-0783.
- As a result of the elemental analysis made on the silver surface, 100% silver was detected on the surface and throughout the section.
- Conductivity of electroless plated silver was calculated as 1.8×10^7 S/m.

REFERENCES

[1] Wu,J. M., Lu,W. Z., Lei, W., and Wang, X. C. Preparation of ZnAl2O4-based microwave dielectric ceramics and GPS antenna by aqueous gelcasting. Mater. Res. Bull., *46,*(9),1485-1489. 2011

[2] Reane, I. M., Iddles, D. Microwave dielectric ceramics for resonators and filters in mobile phone networks. J. Am. Ceram. Soc., *(89)*, 7, 2063-2072. 2006

[3] Abubakarov, A. G., Verbenko, I. A., Reznichenko, L. A., Noykin, Y. M. BSN - Ceramics - Advanced radar-Absorbing material in Conference Proceedings, 159-160. 2017

[4] Narang, S. B., Bahel, S. Low loss dielectric ceramics for microwave applications: A review. J. Ceram. Process. Res., *11*, 3, 316-321. 2010

[5] Wakino, K., Nishikawa, T., Ishikawa, Y. Miniaturization Technologies of Dielectric Resonator Filters for Mobile Communications. IEEE Trans. Microw. Theory Tech., 42,7, 1295-1300. 1994

[6] Wersing,W. Microwave ceramics for resonators and filters. Curr. Opin. Solid State Mater. Sci., *1*, 5, 715-731. 1996

[7] Kishk, A. A., Huang, W. Size-reduction method for dielectric-resonator antennas. IEEE Antennas Propag. Mag., *53*, 3, 26-38. 2011

[8] Oberhammer, J., Somjit, N., Shah, U., Baghchehsaraei, Z. RF MEMS for automotive radar. Handbook of Mems for Wireless and Mobile Applications, 518-549. 2013

[9] Liu, X., Liu, M., Xin, F. Sound absorption of a perforated panel backed with perforated porous material: Energy dissipation of Helmholtz resonator cavity. Mech. Syst. Signal Process., *185*. 2023

[10] Sebastian, M. T. CHAPTER ONE INTRODUCTION. *Dielectric Materials for Wireless Communication.* (1ST Edition) pp. (1-10). Elsevier Science. 2008

[11] Richtmyer, R. D. Dielectric resonators. J. Appl. Phys., *10*, 6, 391-398. 1939

[12] Schlicke, H. M. Discoidal vs Tubular Feed-Through Capacitors. Proc. IRE,*43*, 2, 174-178. 1955

[13] Okaya, A., Barash, L. F. The Dielectric Microwave Resonator*. Proc. IRE, *50*, 10, 2081-2092. 1962

[14] Cohn, S. B. Microwave Bandpass Filters Containing High-Q Dielectric

Resonators. IEEE Trans. Microw. Theory Tech., *16,* 4, 218-227. 1968

[15] Masse, D. J., Pucel, R. A., Readey, D. W.,Maguire, E. A.,Hartwig, C. P. A New Low-Loss High-K Temperature-Compensated Dielectric for Microwave Applications. Proc. IEEE, *59*, 11, 1628-1629. 1971

[16] Plourde, J. K., Linn, D. F. MICROWAVE DIELECTRIC RESONATOR FILTERS UTILIZING Ba2Ti9O20 CERAMICS, 290-293. 1977

[17] Negas,T., Yeager, G., Bell, S., Amren, R. Chemistry and properties of temperature compensated microwave dielectrics. NIST Spec. Publ., 804, 21-37. 1991

[18] Freer, R., Azough, F. Microstructural engineering of microwave dielectric ceramics. J. Eur. Ceram. Soc., *28,* 7, 1433-1441. 2008

[19] Dash, S. K. K., Khan, T., De, A. Dielectric resonator antennas: An application oriented survey. International Journal of RF and Microwave Computer-Aided Engineering. 2017

[20] Plourde, J. K., Ren, C.L. Application of Dielectric Resonators in Microwave Components. IEEE Trans. Microw. Theory Tech., *29*, 8, 754-770. 1981

[21] Marley, P. M., Symes, W., Megherhi, M., Gleason, C. Microwave Materials: Dielectric Compositions for Use in High-Frequency LTCC, Filter, Resonator, and Antenna Applications. IEEE MTT-S International Microwave Symposium Digest, 1438-1441. 2019

[22] Sandhu, M. Y., Hunter, I. C. Miniaturized dielectric waveguide filters. Int. J. Electron., *103*, 10, 1776-1787. 2016

[23] Hattori, J., Wada, T., Kubo, H., Ishikawa, Y. 2GHz band quadruple mode dielectric resonator filter for cellular base station. IEE MTT-S International Microwave Symposium Digest, 2, 933-936. 2003

[24] Singhwal, S. S., Kanaujia, B. K., Singh, A., Kishor, J. Circularly polarized V-shaped dielectric resonator antenna. Int. J. RF Microw. Comput. Eng., *29*, 9. 2019

[25] Zeng, Q., Li, W., Shi, J. L., Guo, J. K., Zuo, M. W., Wu, W. J. A new microwave dielectric ceramic for LTCC applications. J. Am. Ceram. Soc., 89, 5, 1733-1735. 2006

[26] Liu,X. Tunable RF and microwave filters. IEEE 16th Annual Wireless and Microwace Technology Conference, *2015.* 2015.

[27] Kamba, S. *et al.* High frequency dielectric properties of A5B4O15 microwave ceramics. J. Appl. Phys., *89*, 7, 3900-3906. 2001.

[28] Firmansyah, T., Herudin, Kurniawan, F., Denny, Y. R. Multiband microstrip

antenna array with slot and array method for GSM, WCDMA, and LTE. International Conference on Broadhband Communication, Wireless Sensors and Powering. 2018

[29] Ohsato, H. *et al.* Microwave-millimeterwave dielectric materials. Key Engineering Materials, *269,* 195-198. 2004

[30] Liu, H., Yu, H., Tian, Z., Meng, Z., Wu, Z., Ouyang, S. Dielectric properties of (1-x)CaTiO3-xCa(Zn1/3Nb 2/3)O3 ceramic system at microwave frequency. J. Am. Ceram. Soc., *88*, 2, 453-455. 2005.

[31] Huang, C. L., Chen, H. L., Wu, C. C. Improved high Q value of CaTiO3-Ca(Mg1/3Nb2/3)O3 solid solution with near zero temperature coefficient of resonant frequency. Mater. Res. Bull., *36*, 9, 1645-1652. 2001

[32] Hu, X., Chen, X. M., Wu, S. Y. Preparation, properties and characterization of CaTiO3- modified Pb(Fe1/2Nb1/2)O3 dielectrics. J. Eur. Ceram. Soc., *23*, 11, 1919-1924. 2003

[33] KELL, R. C., GREENHAM, A. C., OLDS, G. C. E. High-Permittivity Temperature-Stable Ceramic Dielectrics with Low Microwave Loss. J. Am. Ceram. Soc., *56*, 7, 352-354. 1973

[34] Liu, T., Zhao, X. Z., Chen, W. A/B site modified CaTiO3 dielectric ceramics for microwave application. J. Am. Ceram. Soc., *89*, 3, 1153-1155. 2006

[35] Yin, C. *et al.* NaCa4V5O17: A low-firing microwave dielectric ceramic with low permittivity and chemical compatibility with silver for LTCC applications. J. Eur. Ceram. Soc., 40, 2, 386-390. 2020

[36] Lim, E. H., Pan, Y. M., Leung, K. W. Dielectric resonator antennas. *Handbook of Antenna Technologies*. pp. (955-1000). Springer Singapore. 2016

[37] Tassin, P., Koschny, T., Kafesaki, M., Soukoulis, C. M. A comparison of graphene, superconductors and metals as conductors for metamaterials and plasmonics. Nat. Photonics, *6*, 4, 259-264. 2012

[38] Ohsato, H. Microwave materials with high Q and low dielectric constant for wireless communications. Materials Research Society Symposium Proceedings, 833, 55-62. 2005

[39] Wu,X., Liu, X. Hickle, M. D., Peroulis, Di., Gómez-DÍaz, J. S., Álvarez Melcón, A. Isolating Bandpass Filters Using Time-Modulated Resonators. IEEE Trans. Microw. Theory Tech., *67*, 6, 2331-2345. 2019

[40] Wakino, K. HIGH FREQUENCY DIELECTRICS AND THEIR APPLICATIONS. IEEE, 97-106. 1986.

[41] Jantunen, H., Kangasvieri, T., Vähäkangas, J., Leppävuori, S. Design aspects of microwave components with LTCC technique. J. Eur. Ceram. Soc., *23*, 14,

2541-2548. 2003

[42] US Patent Office. Method of electroless deposition on a substrate and catalyst solution therefor (US3011920A). Shipley Co Inc: Jr Charles R Shipley.1960.

[43] US Patent Office. REDUCING ELECTROLESS SILVER PLATING SOLUTION AND REDUCING ELECTROLESS SILVER PLATING METHOD (US20140242288A1). C Uyemura and Co Ltd: Daisuke Hashimoto, Kota Kitajima, and Aki. 2014

[44] Sharma, A. Cheon, C.-S., Jung, J. P. Recent Progress in Electroless Plating of Copper. J. Microelectron. Packag. Soc., *23*, 4, 1-6. 2016

[45] Barker, B. D. Electroless deposition of metals. Surf. Technol., *12*, 1, 77-88. 1981

[46] S. B. Lyon, Corrosion of noble metals. *Shreir's Corrosion*. pp. (2205-2223). Elsevier.2010

[47] Walsh, F. C. Electrode reactions in metal finishing. Trans. Inst. Met. Finish., 69, 3, 107-110. 1991

[48] Kepp, K. P. Chemical Causes of Metal Nobleness. ChemPhysChem. 2020

[49] ASTM. Standard Specification for Electrodeposited Coatings of Silver for Engineering Use (B700-20). 2020

[50] ASTM. Standard Specification for Electrodeposited Coatings of Silver for Engineering Use (B700-20). 2020

[51] Srinivasan, G., Murcko, R., Srihari, K. Evaluation of secondary wire bond integrity on Ag plated and ni/pd based lead frame plating finishes. Proceedings of the ASME InterPack Conference, 1, 283-292. 2010

[52] Malone, G. Electroforming. *ASM Handbook : Volume 5 - Surface Engineering*. p. (647). 1993

[53] Renhart, P., Summer, F., Grün, F., Posch, C., Eder, A. The tribological performance of silver in aircraft turbine load cases. Tribol. Int., *163*. 2021

[54] Kiełbasiński, K. *et al.* New technology of silvering aluminium busbar joints with the use of printable paste containing nano-size Ag particles. J. Mater. Sci. Mater. Electron., *26*, 3, 1832-1837. 2015

[55] Surface Engineering of Aluminum and Aluminum Alloys. *ASM Handbook : Volume 5 - Surface Engineering* pp. (2123–2124). 1993

[56] Shukla, S., Gomathi, N., George, R. Autocatalytic silver-plating of aluminium radio frequency waveguides with autocatalytic nickel as the undercoat for space applications. Surf. Topogr. Metrol. Prop., *2*, 4. 2014